CCFE
CULHAM CENTRE FOR FUSION ENERGY

UK Atomic Energy Authority

UKAEA-CCFE-PR(23)103

R. Scannell, H. Liu, E. Mukhin, E. Yatsuka, A. Gorbunov, L. Giudicotti, G. Kurskiev, J. Chen, M. A. Van Zeeland, D. Finkenthal, R. Imazawa, D. Brower, A. Sirinelli, T. Akiyama, T. Carlstrom, D. Johnson, M. Lesher, C. Watts, M. Bassan

ITER Physics Basis Update Chapter 6: Laser Aided Diagnostics

ITER Physics Basis Update Chapter 6: Laser Aided Diagnostics

R. Scannell, H. Liu, E. Mukhin, E. Yatsuka, A. Gorbunov, L. Giudicotti, G. Kurskiev, J. Chen, M. A. Van Zeeland, D. Finkenthal, R. Imazawa, D. Brower, A. Sirinelli, T. Akiyama, T. Carlstrom, D. Johnson, M. Lesher, C. Watts, M. Bassan

This is a preprint of a paper submitted for publication in Nuclear Fusion

ITER Physics Basis Update

Chapter 6: Laser Aided Diagnostics

R. Scannell[1], H. Liu[2], E. Mukhin[3], E. Yatsuka[4], A. Gorbunov[5], L. Giudicotti[6], G. Kurskiev[3], J. Chen[10], M. A. Van Zeeland[7], D. Finkenthal[8], R. Imazawa[9], D. Brower[10], A. Sirinelli[11], T. Akiyama[7], T. Carlstrom[7], D. Johnson[12], M. Lesher[7], C. Watts[11], M. Bassan[11]

[1] UKAEA, Culham Science Centre, Abingdon, OX14 3DB, UK
[2] Institute of Plasma Physics, Chinese Academy of Sciences, Hefei, Anhui 230031, People's Republic of China
[3] Ioffe Physical Technical Institute, 26 Polytechniheskaya, 194021 St Petersburg, Russian Federation
[4]JAEA, 801-1 Mukoyama, Naka, Ibaraki 311-0193, Japan
[5]NRC Kurchatov Institute, Moscow, 123182, Akademika Kurchatova, sq 1, Russia
[6] Padova University, Department of Physics and Astronomy, Via Marzolo 8, 35131 Padova, Italy
[7] General Atomics, P.O. Box 85608, San Diego, California 92186-5608
[8] Palomar Scientific Instruments, San Marcos, California 92069, USA
[9] National Institutes for Quantum and Radiological Science and Technology, Naka, Japan
[10] Department of Physics and Astronomy, University of California Los Angeles, Los Angeles, California 90095, USA
[11] ITER Organization, Route de Vinon sur Verdon, CS 90 046, 13067 St. Paul Lez Durance Cedex, France
[12] Princeton Plasma Physics Laboratory, PO Box 451, Princeton, NJ 08543, USA

E-mail: rory.scannell@ukaea.uk

Received xxxxxx
Accepted for publication xxxxxx
Published xxxxxx

Abstract

An overview of the laser diagnostics to be implemented on ITER is provided in this paper. This includes descriptions of the Thomson scattering in the Core, Edge and Divertor regions, polarimetry and interferometry diagnostics used for measuring plasma density and also measurements of Helium density in the divertor using Laser Induced Flourescence. Techniques which can allow improvements on current measurements are also addressed in particular expanding poloidal polarimetry measurements to measure field fluctuations and proposed use of dispersion interferometery which has a number of advantages over existing methods. This paper identifies particular areas where further research and testing on existing tokamaks is useful even at this advanced stage to inform the design of diagnostics for ITER. Outstanding areas of concern for the implementation of laser diagnostics, in particular with a view to reliable operation are identified.

Keywords: lasers, diagnostics, ITER, Thomson, polarimetry, interferometry

Abbreviation	Meaning
AR	Anti-Reflection
APD	Avalanche PhotoDiode
CCR	Corner Cube Reflector
CM	Cotton-Mouton
CPTS	Core Plasma Thomson Scattering
CRM	Collisional Radiative Models
DAQ	Data AcQuisition
DFW	Diagnostic First Wall
DI	Dispersion Interferometry
DTS	Divertor Thomson Scattering
ECCD	Electron Cyclotron Current Drive
ECE	Electron Cyclotron Emission
ECRH	Electron Cyclotron Resonance Heating
EFIT	Equilibrium FIT
EQE	Effective Quantum Efficiency
ETS	Edge Thomson Scattering
FIR	Far infra-red
FPGA	Field Programmable Gate Array
FWHM	Full Width at Half Maximum
HeNe	Helium Neon
LHD	Large Helical Device
LIDAR	Light Imaging Detection and Ranging
LIF	Laser Induced Flourescence
LIQ	laser-induced quenching
Nd:YAG	Neodymium doped Yttrium aluminum garnet
Nd:YLF	Neodymium doped Yttrium lithium fluoride
OPO	optical parametric oscillator
PEM	Photo-Elastic Modulator
PoPola	Poloidal Polarimeter
QCL	quantum cascade laser
RCP	Right Circular Polarisation
SNR	Signal to Noise Ratio
SOL	Scrape off layer
TIP	Tangential Interferometer Polarimeter
TS	Thomson Scattering
VDF	Velocity Distribution Function

Table 1. Abbreviations

1. Introduction

The required plasma measurements to make ITER a success, of which laser diagnostics are a crucial component, flow from the ITER overall Project Requirements document (Chiocchio & Grosset, 2020). The Project Requirements document details what must be achieved by the ITER plant based on the underlying physics. From this document, the particular requirements for individual diagnostic systems are derived and detailed in the ITER diagnostics requirements document (Reichle, Ulysse, Casoria, & Turnyanskiy, 2020). The means of meeting the measurement requirements for ITER was intially addressed in (Editors, 1999) for the full diagnostic set and in particular for laser diagnostics in section 3.3 of this document. Further progress in diagnostics systems with specific examples was last set out in 2007 and published in (Donne, Costley, & Barnsley, 2007).

This current paper details the status of the various laser diagnostics that will be used to meet the measurement requirements. Each section contains links to relevant background to properly introduce each diagnostic system.

As well as describing the various diagnostic systems themselves relevant techniques are also discussed. Polarimetric and dual laser Thomson scattering techniques which are particularly useful for TS systems on ITER are introduced. Neither are routinely employed on existing tokamaks but they are being tested with a view to application on ITER. The polarimetric technique in particular has developed considerably since the last update to the ITER physics basis.

The LIF diagnostic which will be integrated into the divertor Thomson scattering diagnostic is a new advance also relative to the ITER physics basis published in 2007. The Toroidal Interferometer Polarimeter system, which is planned to be used for real time density control at ITER, has recently been prototyped and deployed in a test capacity at DIII-D. While the PoPola diagnostic has been in the ITER diagnostic set for some time, it's proposed use for magnetic fluctuation measurements and plasma vertical control are a recent development. The final diagnostic discussed is the Dispersion interferometer which is another recent innovation. Due to its configuration, it is highly resistant to vibrations making it a very robust measurement tool and motiviating its application for ITER.

2. Core Thomson Scattering

The ITER Core Plasma Thomson Scattering diagnostic was originally envisaged as a LIDAR design (Walsh, 2006). However, following a proposal the design has been modified to follow a conventional TS layout, shown in figure 1, which operates at high scattering angle. A detailed design trade-off between the LIDAR and conventional design solutions was considered in making this decision. Some of the main factors motivating a conventional design were easier availability of detectors and laser, higher spatial resolution and longer beam dump lifetime.

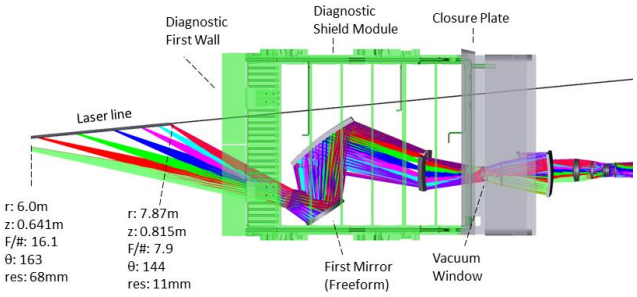

Figure 1 – Optical design of CPTS diagnostic. The first and second and sixth mirrors from the plasma (shown in red) are free form. The approximate parameters for the furthest in and out most measurement points are indicated.

The CPTS diagnostic must meet requirements on its performance which derive from the ITER project requirements (Chiocchio & Grosset, 2020). The CPTS diagnostic has a number of common elements with the edge TS diagnostic, since both systems are conventional systems based on Nd:YAG lasers operating at high scattering angle. Particularly important common elements include the beam dump (Yatsuka, 2013) (Yatsuka, Enhancement of resistance against high energy laser pulse injection with chevron beam dump, 2015) and solutions for laser beam combination (Yatsuka, Development of laser beam injection system for the Edge Thomson Scattering (ETS) in ITER, 2016) as well as laser and collection optics alignment. Particularly important differences with the edge system are the more challenging optical labyrinth (neutron attenuation) trade off for CPTS, larger first aperture and hence shutter requirement for the CPTS and requirement for the CPTS to measure to higher electron temperature and hence lower wavelength.

The main components of the proposed system are a 5J, 100Hz, 4ns laser system, envisaged to consist of at least 2 lasers for redundancy, an optical system collecting at F/16.4 at r/a~-0.1 at ~160degrees varying to F/7.6 at r/a~0.85 at ~130degrees. The CPTS system design has capability for measurement of 'p' as well as 's' polarised scattered light, originally proposed by (Orsitto & Tartoni, 1999) and detailed further in (Giudicotti, 2016). The proposed CPTS system also includes a 1319nm 10Hz 2J laser operating in conjunction with the main 1064nm laser. This multi-laser approach has been suggested for each of the ITER TS diagnostics motivated by requirements for calibration and to reach high electron temperature, a recent consideration has been made in (Kurskiev, 2015).

In order to achieve good optical performance and neutron shielding, freeform optical elements have been included in the new optical design. These are challenging to implement, in particular in conjunction with the requirement for a mirror cleaning system for the first mirror but promise benefits in performance. Considering simulated ITER profiles, density and temperature gradients imply that higher spatial resolution is required in the mid-radius and outboard region than in the core. This higher resolution is naturally achieved for a fixed fibre bundle size due to the change in collection F/#.

The main challenges facing the diagnostic are in terms of survivability of plasma facing components in the harsh operating environment, the long duration of 4700hours of operations and the inaccessibility during this operating period. Some of these key engineering challenges are listed below;

- Survivability of the First Mirror in a harsh and unknown plasma environment where deposition is expected (Mukhin, 2012)
- Demonstration of a Mirror cleaning system compatible with the first mirror (Litnovsky, 2010), particularly if free form.
- Engineering implementation of a mirror protection shutter at high reliability. This shutter must contain cooling channels.
- Active Alignment of the scattering lasers to the beam dump to maintain sub-cm alignment during plasma pulses.
- Survivability of the laser beam dump.

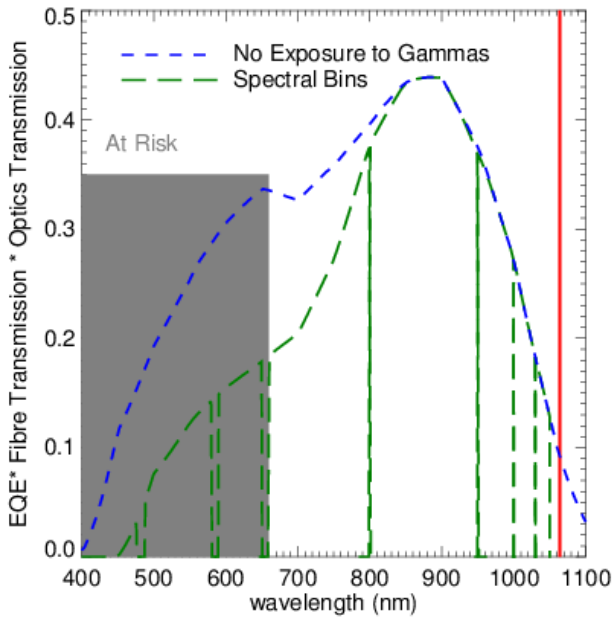

Figure 2 – Optical transmission of the CPTS diagnostic including full information of spectral transmission of the various collection optic elements, the detector EQE and optical fibre transmission. The

optical fibre transmission includes expected degradation for the 'intermediate' OH fibre after 10kGy of radiation. The 'at risk' region, which may suffer further transmission losses is highlighted.

As well as diagnosing electron temperature profiles more generally, one of the particular key goals of the CPTS diagnostic is to measure the peak core T_e value. This peak core T_e will be an important indicator of ITERs success. This implies that the diagnostic must measure to the lowest possible wavelength ~400nm see figure 2. There are a number of factors that make measurement at this very low wavelength difficult, in particular first mirror reflectivity losses are expected to be in this region, as will transmission losses for optical fibres and Cerium doped lens elements in the interspace. Also there is significant line emission in the lower wavelength region. However, there are new diagnostic advances that should aid the CPTS in these crucial measurements and help distinguish from any spectral transmission uncertainty at the edge of the wavelength region. These advances are 'Polarimetric' Thomson scattering, measuring the polarisation of the scattered light and use of a 1318nm Nd:YAG laser. The theoretical concepts behind these techniques have been further developed in the last few years. Polarimetric and Two-wavelength Thomson scattering are now being prototyped and tested on existing machines.

3. Edge Thomson Scattering (ETS)

ETS has an important specification to measure the region of r/a> 0.85 with a spatial resolution of 5 mm in order to measure the steep electron density and temperature gradient in H-mode discharges. The electron temperature range covered by ETS is 0.05-10 keV. This temperature range is measures from 590-1060 nm with 6-channel polychromator spectrometers. To detect enough photons, F-number of the ETS collection optics is F/9. While using such a bright optical system, it is a challenge to minimize chromatic aberration over the above-mentioned wavelength band and to be compatible with radiation shielding. The key engineering challenges are the same as the five listed in the CPTS section.

The optical path of the collection optics forms a labyrinth in the port plug to pass the collected light and to shield neutrons from the plasma. No lens is used in the port plug to avoid fracturing of glass due to vibrations during plasma disruptions. The collection optics are capable of collecting light from a normalized minor radius range between 0.80 and 1.08. The outermost line of sight (LOS) corresponds to the face of the diagnostic first wall (DFW) (Yatsuka, 2018). In order to suppress aberrations, the angle of incidence on the curved mirror was made as small as possible. Figure 3 shows the configuration of the ETS collection optics. Considering the radiation environment near the port plug, it is desirable that the field of view of the collection optics can be adjusted without human intervention. Light propagating in the opposite direction from the optical fiber hits the bracket near the upper port. By observing the vignetting of spots projected on the blanket, the relative relationship between DFW and the observation position can be maintained.

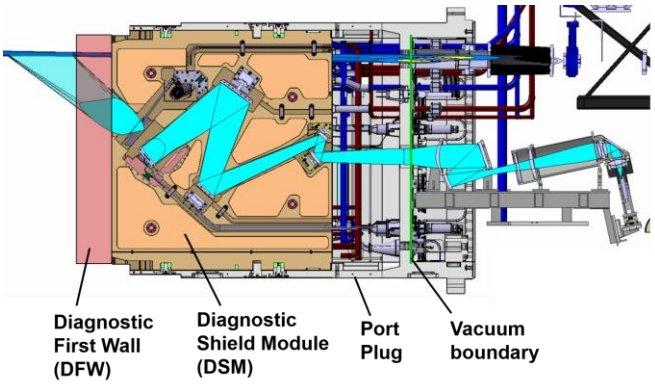

Figure 3 – Configuration of the ETS collection optics. Inside the port plug, it consists of only mirrors, and outside the port plug, it consists of mirrors and lenses.

The laser beam dump is mechanically installed on the inner blanket. The space provided for the beam dump is 60 mm wide, 115 mm high and 77 mm deep, including a flange for mounting on the blanket. If the laser beam dump fails, the entire blanket must be replaced by remote handling maintenance equipment. In order to reduce the risk of laser beam dump failure, the beam diameter should be as large as possible. For this purpose, the beam has to always be incident on the center of the laser beam dump. ETS achieves a temporal resolution of 100 Hz by alternately firing two 50 Hz laser beams. The use of two lasers enables us to perform the Thomson scattering measurements at a temporal resolution of 50 Hz in case that one of the laser systems stops functioning. In order to maximize the light receiving surface of the laser beam dump, allow use of two laser beams, and suppress the streaming of neutrons along the beam optical path, it is necessary to align the two beams coaxially. Since the scattering angle is about 140 degrees and the measured electron temperature is up to 10 keV, the depolarization of scattered light is at most a few percent. In order to improve the ratio of Thomson scattered light to the background light of randomly polarized light, a polarizer is installed in the collection optics. The functional requirements for laser incidence and laser beam dump are summarized below. The two horizontally polarized beams must be coaxial and always incident at the center of the laser beam dump. The laser beam dump needs to survive for a long time under the severe heat load of ITER.

A rotating half-wave plate provides a lossless method for combining beams together with stable beam pointing. The polarization extinction ratio of the combined beams can exceed 1000 (Yatsuka, 2017).

In order to inject the probing beam into the center of the laser beam dump, a method for detecting the beam position is required. The beam position at the laser beam dump is monitored by four alignment laser beams which propagate parallel to the probing Nd:YAG laser beam and imaging systems installed outside the port plug (Yatsuka, Development of laser beam injection system for the Edge Thomson Scattering (ETS) in ITER, 2016).

ITER is scheduled to operate for about 4700 hours of plasma, and when the beam is incident at a repetition rate of 100 Hz, the number of pulses on the beam dump will be on the order of 10^9. The laser beam dump is made of molybdenum alloy and is designed to withstand high heat loads. To reduce the risk of laser damage, the internal structure of the laser beam dump has been proposed as shown in Figure 4 (Yatsuka, 2013). It has a structure in which a large number of 0.5 mm molybdenum alloy sheets bent at several points are arranged in parallel with a clearance of 0.6 mm. In this structure, S-polarized beams are incident at a large angle of incidence (wide area). Therefore, the beam energy absorption density can be reduced to about 1/20 as compared with the case where the angle of incidence is 0. It has been experimentally shown that this structure is advantageous for the survival of the beam dump (Yatsuka, Enhancement of resistance against high energy laser pulse injection with chevron beam dump, 2015), and it has been confirmed that it can be manufactured (Yatsuka, 2018).

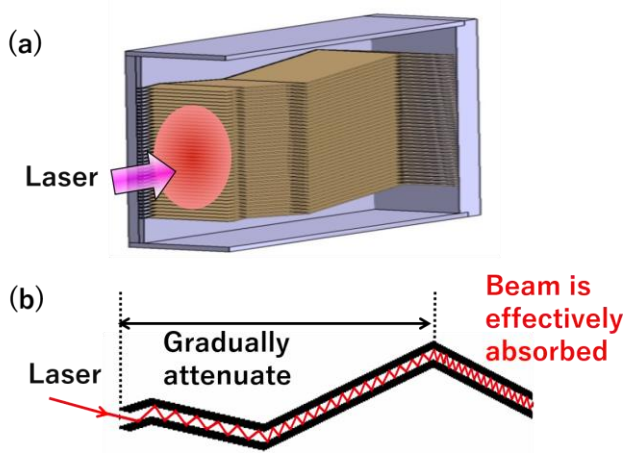

Figure 4 – (a) Bird's eye view and (b) concept of the laser beam dump.

In order for the laser beam to be injected into the plasma, it passes through a vacuum window. The vacuum window is also the confinement boundary for tritium and beryllium. Vacuum windows are expected to be exposed to a total gamma dose of several MGy. A 10 MGy gamma ray irradiation was performed on fused silica windows with the antireflection coating, and then a laser injection test was performed. It was confirmed that the laser-induced damage threshold did not deteriorate (Yatsuka, 2020).

4. Multi-Color Thomson Scattering

In the case of core TS system the main candidates for the calibration laser are: second harmonic of Nd:YAG 532 nm and alternative lasing Nd:YAG wavelengths 946 and 1320 nm. Using different probing wavelengths also leads to an effective increase in the number of spectral channels (see FIG. 5). This can enhance the diagnostics capabilities if the electron velocity distribution function (VDF) deviates from a Maxwellian that can take place under a strong ECRH/ECCD (Kurskiev, 2015). For the temperature range 0.5-40 keV the calibration coefficient for each channel can be determined with an accuracy of about 10%. This is not enough since the calibration coefficients should be determined with an accuracy not worse than 1-2%. Therefore, averaging over a hundred pulses is required, that poses a problem for usage of three level Ruby laser with a suitable wavelength of 694 nm. Due to the extremely wide T_e range there is no optimal choice of a supplementary laser, each choice has its own pros and cons. The use of both additional 1320 nm and 946 nm seems to be preferable because this a) allows successful operation when the spectral sensitivity changes quickly; b) allows calibration of the system in the entire temperature range; c) improves the accuracy in the case of non-Maxwellian electron VDF. Usage of 1320 nm laser is sufficient for system calibration and accuracy improvement both for high T_e measurements and non-Maxwellian VDF. The Nd:YAG 532 nm laser can be recommended for system calibration using only special ITER regimes within the limited Te range. The benefit of additional lasers can be summarized as follows (Kurskiev, 2015):

- Nd:YAG 1320 nm pro: significantly increases accuracy for high temperature measurements T_e>10 keV, spectral calibration is possible for T_e>1.5 keV, accuracy increase in the case of non-Maxwellian electron VDF. Nd:YAG 1320 nm contra: the laser is not yet commercially available, poor T_e accuracy in double laser mode for Te <1.5 keV, different spectral channels should be calibrated at different temperatures.

- Nd:YAG 936 nm pro: calibration is possible in the full temperature range, could be used as the main laser in emergency case. Nd:YAG 936 nm contra: bad Te accuracy in double laser mode for T_e >10 keV, useless in non-Maxwellian electron VDF case, different spectral channels should be calibrated at different temperatures.

• Nd:YAG 532 nm pro: availability, all channels can be calibrated at one temperature, but this range is very short. Nd:YAG 532 nm contra: sufficient T_e accuracy in double laser mode only for 6keV < T_e < 15keV range, spectral calibration is possible only for 8keV < T_e < 20keV, useless in non-Maxwellian electron VDF case.

Measurements of T_e as high as 40 keV in the plasma core of a large fusion device such as ITER encounter a number of issues. The most reliable techniques that can be used are Thomson scattering and electron cyclotron emission intensity (ECE) diagnostics. In case of ECE a large relativistic and Doppler broadening will have a significant impact on spatial resolution of the measurements. As for example for regimes with core $T_e(0)$=30 keV the required spatial resolution a/30 (where a is the reduced small radius of the plasma) will be possible only for the outer region of the plasma column, r/a > 0.5 (Bartlett, 1996) (Vayakis, 2006). In case of TS scattering diagnostics, the main issue is a significant blue shift for backscattering geometry, see FIG. 6, while the operational wavelength range is bounded on the blue side (400-500 nm) due to the collection optics transmission at and the strong background radiation (Kurskiev, 2015) (Bassan, 2016). The problem will be made worse due to the darkening of the collection optics and fibres under strong neutron and gamma irradiation. In the worst case the lower wavelength limit can be shifted to 700 nm thus limiting the TS system dynamic range to a few keV (Kurskiev, 2015) (Scannell, 2017). At high T_e the σ_{Te}/T_e values expected from the 1064 nm laser are limited by ability to determine the shape of the spectrum, in particular it becomes more difficult to distinguish between increasing temperature and density. The possible solutions to this problem are: alternative geometry with lower scattering angle, depolarization measurements (see section 2 for details) and using an additional probing wavelength shifted deeper to near infrared range. Nd:YAG lasers have emission lines at 1319 nm and 1338 nm. Using large scale Nd:YAG crystals together with high-power laser diode pumping allows one to realize such lasers operating with the pulse energy as high as 1–2 J and a repetition rate of 50–100 Hz. At present a TS system is currently being prepared for experiments at Wendelstein 7-X (Pasch, 2018) using a 1319nm laser. The main advantage of such approach is the effective shift of spectral channels relative to the TS spectrum shape closer to the position of the maximum, see FIG. 5. It allows to significantly reduce the temperature and density error correlation for 20–40 keV for a 1319 nm laser in comparison with a 1064 nm laser thus increasing the measurement accuracy of n_e and T_e. Moreover, the other advantage of this technique is the inherent in-situ spectral calibration.

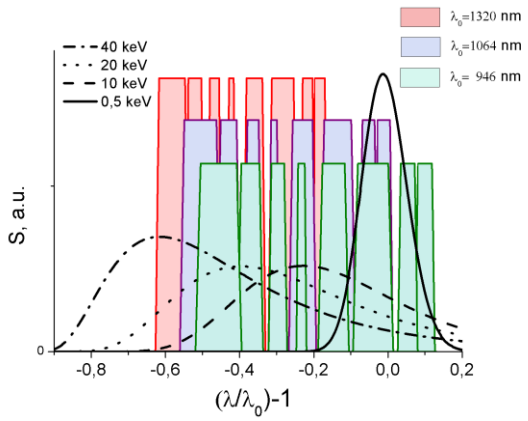

FIG. 5. Effective increase in the number of spectral channels for the different YAG probing wavelength in comparison with TS spectra for the different T_e.

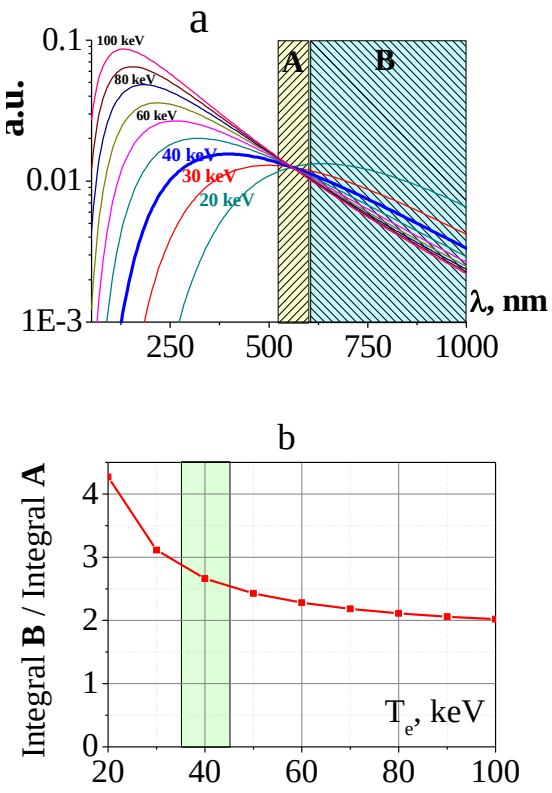

FIG. 6. a) Thomson scattering spectra for scattering angle θ=170° and T_e = 20-100 keV , the spectra normalized by integral in the wavelength range "A". b) The ratio of integrals in ranges "A" and "B" depends on T_e, however for high T_e the uncertainty drastically increases due strong interdependence of T_e and n_e.

5. Polarimetric Thomson Scattering

Polarimetric Thomson scattering (TS) is an advanced technique for the analysis of TS spectra that exploits the depolarization of the scattering radiation (Orsitto & Tartoni, 1999). This is an effect barely noticeable in present-day fusion plasmas, but becomes important in plasmas with T_e of the order of tens of keV, as it is expected in the high T_e regimes of ITER (Bassan, 2016). Polarimetric TS has been suggested as a method to mitigate the loss of accuracy of the ITER Core Plasma Thomson Scattering (CPTS) system due to the fact that in the high T_e regimes of ITER the spread of the TS spectrum exceeds considerably the spectral region considered to be useful for the detection of the TS signal (Giudicotti, Depolarization measurements in ITER Core Plasma TS, 09-06-2017). This is the wavelength region 650 nm < λ < 1060 nm and its limits are determined by the drop of the silicon avalanche photo diodes quantum efficiency on the long wavelength side and by the region of high background plasma light on the low wavelength side. In addition the spectral region 400 nm < λ < 650 nm is also considered 'at risk' of transmission loss due to windows and fiber optics from neutron irradiation. For this reason, when the plasma T_e is high and the TS spectrum spreads outside the useful detection region, the reconstruction of the shape of the TS spectrum becomes difficult and the expected measurement errors increase. Polarimetric TS provides a method to mitigate this, contributing to keeping the T_e and n_e measurement errors low also in the high T_e regime (Giudicotti, 2016) (Giudicotti, 2017). Recently the depolarization of TS radiation has been experimentally observed in JET (Giudicotti, 2018).

In order to describe the polarization properties of the scattering radiation it is convienient to use the Mueler calculus (Goldstein, 2003). Theory shows (Giudicotti, 2017) that the radiation scattered by a high T_e, relativistic plasma is partially polarized and its Stokes vector can be written as $\boldsymbol{S} = C_{PL}\boldsymbol{S}_{PL} + C_{NP}\boldsymbol{S}_{NP}$ in which $\boldsymbol{S}_{PL} = (1, s_1, s_2, s_3)$ and $\boldsymbol{S}_{NP} = (1,0,0,0)$ are unit Stokes vectors representing the completely polarized and the unpolarized components of the radiation and C_{PL} and C_{NP} are their intensity coefficients. The quantity $P = C_{PL}/(C_{PL} + C_{NL})$ is the degree of polarization and $D = 1 - P$ is conventionally called "depolarization" (Segre, 2000). Both are functions of the electron temperature only. The Stokes vector of the wavelength integrated scattering radiation is computed as $\boldsymbol{S}(T_e, q) = \boldsymbol{M}(T_e, q)\boldsymbol{S}_{IN}$ where $\boldsymbol{S}_{IN}$ is the Stokes vector of the incident laser beam and $\boldsymbol{M}(T_e, q)$ is the Mueller matrix of TS (Parke, 2014). The scattering signal detected in a given spectral interval can be calculated from the spectral Stokes vector $\boldsymbol{S}_S(\lambda, T_e, q,) = \boldsymbol{M}_S(\lambda, T_e, q)\boldsymbol{S}_{IN}$ in which $\boldsymbol{M}_S(\lambda, T_e, q)$ is the spectral Mueller matrix of TS that can be calculated either numerically (Segre, 2000) or by a semianalytic method (Mirnov, 2016) (Mirnov, 2017). Note that these expressions are valid for any polarization state of the incident laser beam. Let's now consider these quantities for TS from an ITER plasma. Fig. 7 shows the dependence from T_e of the intensities CPL and CNP and of the degree of polarization P of the scattering radiation from a position near the center of the scattering region in the ITER core plasma.

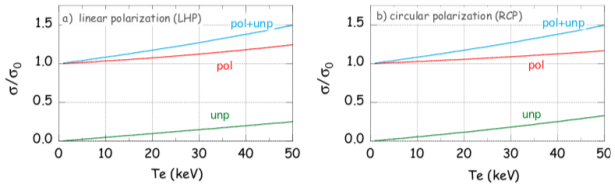

Figure 7. Intensity of the scattering signal (integrated over the full solid angle) as a function of T_e, for an input laser beam with linear and circular polarization. The intensity I is normalized to its value I_0 for a non-relativistic plasma (T_e approaching 0.) The completely polarized and the unpolarized components are also shown. At any T_e the total intensity I is identical for the two input polarizations and increases up to $I = 1.38\ I_0$ for T_e = 40 keV. The intensity of the unpolarized component is higher for a circularly polarized input beam, reaching $0.25\ I_0$ at T_e = 40 keV compared to $0.20\ I_0$ for a linearly polarized input beam.

Note that the unpolarized component increases steadily with T_e and at T_e = 40 keV accounts for up to 20% and to 25% more intensity for an input beam with linear (as usual) or circular polarization, respectively. Since the depolarization occurs in the same way at any wavelength, then P is only a function of T_e. Polarimetric TS allows the determination of T_e by measuring P. The technique can be implemented in any spectral interval and therefore does not suffer from limitations of the useful detection range.

The best way to exploit this depolarization effect in ITER is to include an additional polarimetric channel into a conventional filter polychromator as in Fig. 8 (Giudicotti, 2017)

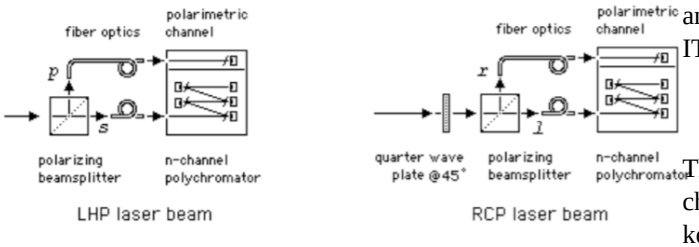

Figure 8. Layout of a TS detection scheme including n spectral and one polarimetric channel. If the input laser beam has linear polarisation as usual, the quarter wave in input is not necessary and the scattering light is separated into the two linear "s" and "p" polarizations. If the input laser beam has right circular polarisation, then the quarter-wave plate at 45˚must be added to separate the scattering light into left "l" and right "r" circular polarisations.

The purpose of this polarimetric channel would be to detect the component of the scattering radiation with the polarization perpendicular to that of the incident laser beam, covering a spectral region as large as possible within the useful detection range. This will provide an additional signal that, contrary to those of the conventional spectral channels, will be increasing with T_e, thus contributing to reducing the measurement error in the high T_e range. In Fig. 9 we show the expected effect of such a polarimetric channel on the accuracy of the measured T_e in ITER assuming that it has the same spectral extension of the full set of spectral channels (Giudicotti, 2017)

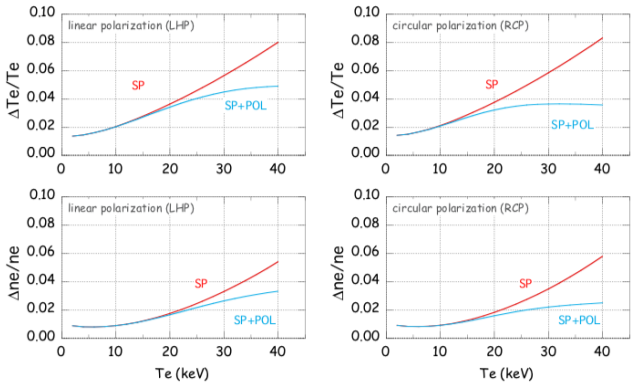

Figure 9. Relative error on T_e and n_e expected using the spectral channels only and with the addition of a polarimetric channel, for linear and circular input polarization in the ITER CPTS. We assumed ne = 5 x 10^{19} m^{-3}, laser energy in the plasma volume E = 3.2 J, collection optics solid angle Omega = 3.14 x 10^{-3} sr (F/9.8), scattering length L = 48 mm, scattering angle theta = 159˚, APD excess noise factor k = 2.5 and no plasma light. The solid angle, scattering length and scattering angle are those of the measurement position in ITER at R = 6.2 m.

These calculations show that the inclusion of the polarimetric channel becomes significant at about 20 keV and at T_e = 40 keV can decrease the T_e and ne measurement errors by about 30% and 50% for an incident laser beam with linear and circular polarization, respectively. In these calculations the possibility of performing TS with a circularly polarized laser beam has been considered. In fact, in TS from a plasma, an incident beam with polarization different from linear perpendicular to the scattering plane has never been done. The reason is that this is the input polarization that maximizes the scattering signal for any scattering angle. However in the almost backward scattering condition of ITER the difference between the scattering signal detected with linear and circular polarizations is hardly appreciable. In fact Fig. 9 shows that the accuracy of the spectral measurement is virtually the same at low T_e whereas the inclusion of a polarimetric channel is more effective at high T_e if the scattering is performed with a circularly polarized laser beam. In ITER however a polarizer, either linear or circular, depending on the polarization of the laser beam, must be inserted in the collection optics, to separate the two polarization components before the fiber optic bundles, as these will destroy the polarization of the scattering light (Scannell, 2017) (R & M, 2018). Such a polarizer must be sufficiently achromatic to operate on the entire detected spectral range and compliant with the requirement of neutron irradiation. A problem that may arise with an input circular polarization is due to the damage threshold of the laser beam dump, whose design was specific for a linearly polarized laser beam (Vayakis & Scannell, 2017). Except for this, polarimetric TS with a circularly polarized input beam may be a real option in ITER.

There are two possible schemes by which a polarimetric measurement may be implemented in ITER. The first is that shown in fig. 8. In this case however a double set of fiber optics bundles is necessary. A second possibility is to use a double laser pulse technique, in which two laser pulses with different polarizations either linear horizontal/vertical or circular right/left are sent on the same path into the plasma with a small time delay. In this way only a single fiber bundle is necessary and also the polarimetric channel can be omitted because the unpolarized component will be measured by the same set of spectra channels on the second laser pulse. In this case however it is necessary to measure the power of the two pulses with good accuracy, and also introducing a beam dump of a different design. In conclusion, including a measurement of the unpolarized component of the TS signal may effectively improve the

accuracy of the TS measurements at high T_e in the ITER CPTS system, counteracting the adverse effect of the limited detection spectral range.

6. Divertor Thomson Scattering

The ITER Divertor Thomson Scattering measures T_e and n_e in the outer divertor leg providing the link between upstream and target parameter measurements (e.g. from Langmuir probes). The diagnostic Measurement Requirements are presented in Table 2. At the very low temperatures, corresponding to the region in which strong recombination and thus divertor plasma detachment will occur the requirement on measurement accuracy is reduced. This is reasonable in the sense that one of the most important roles of the DTS will be to provide experimental evidence that strong recombination is occurring in the target vicinity and to validate plasma boundary code simulations of the detachment behaviour. Since the recombination rate increases more rapidly in the region with T_e below ~0.5 eV in comparison with the interval ~0.5-1.0 eV, it suffices for code validation that experiments provide a measurement, which can distinguish roughly between these regions (Mukhin E. , 2014).

Table 2. DTS measurement requirements

	Coverage	Frequency	Accuracy
n_e	10^{19} - 10^{22} m^{-3}	50 Hz	20%
T_e	1-200eV	50 Hz	20%
	0.3-1eV		0.2eV

The required temporal resolution is based on particle confinement times in the divertor plasma. In ITER, this timescales equate to ∼10 ms defining the minimum timescale upon which 'global' changes might be expected in the divertor plasma (not including, of course, very fast turbulent processes occurring on small spatial scales). The baseline time resolution of the divertor TS system of 20 ms (50 Hz) seems reasonable, especially given the possibility of achieving, if necessary, a factor of two higher resolution (10 ms) through simultaneous application of the spare laser system. The DTS optical layout uses crossed probing and viewing beams with front-end laser launcher located beneath the divertor cassettes. The laser chords (see Figure 10) enter along the bottom of the divertor cassette and, then, travel upwards into the outer divertor SOL, passing through ~20 mm gap between adjacent divertor cassettes. Several interchangeable probing chords with common collection optics improve the diagnostic reliability, proving fast change of probing chords starting from different front-end laser mirrors.

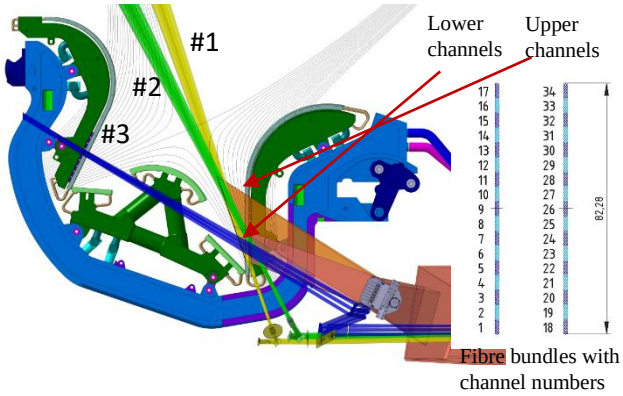

Figure 10. Relative location of DTS probing chords in outer divertor leg and spatial channel arrangement on two fibre bundles corresponding to lower and upper spatial channels.

Laser chords #1 are very close to the separatrix, coinciding with the main stream to the outer divertor leg, and are the most informative for detachment monitoring and control. Laser chords #2 and # 3 are less informative but are launched from mirrors located further from the outer divertor target but better protected from plasma interactions.

The standard processing of the TS spectrum assumes that the spectrum width depends on T_e, while the total scattered signal intensity is linearly proportional to n_e. When studying a sufficiently dense and cold divertor plasma the Debye length approaches the differential scattering vector and the deviation of the TS spectral shape from Gaussian becomes very pronounced (Mukhin E. , 2019). The intended processing of TS spectra is fitting the measured spectra with theoretical expectations, estimating the n_e and T_e measurement errors from simple analytical equations (Kurskiev, 2015). The DTS measurement capabilities were assessed by estimation of n_e and T_e relative errors for TS spectra with pronounced collective effects using the following algorithm:

(a) estimation of TS signals in spectral channels based on the known engineering parameters;

(b) multiple inverse problem solution (103 runs) recovering T_e and n_e from the TS signals simulated for given n_e and T_e with allowance for random deviations , where k ~2.5 APD excess noise, N_i and N_{bg} i - number of signal and background photoelectrons in ith spectral channel, N_{amp}~ 50 contribution of the detector and amplifier noise reduced to the input of detector (minimal error of the scattered signal was assumed as 2.5%, taking into account probable systematic errors due to calibration);

(c) estimation of the T_e and n_e standard deviations from the obtained distributions of T_e and n_e.

The assessed relative errors of the measured T_e and n_e for the probing chord #1 are summarized in Figure 11. Figure 11 a, b shows that the measurement errors of both T_e under n_e = $2x10^{20}$ m^{-3} and of n_e under T_e = 0.3 eV satisfy the requirements (plasma parameters near strike point). The same analysis for plasma parameters typical for upper part of the divertor leg is presented in Figure 11 c, d).

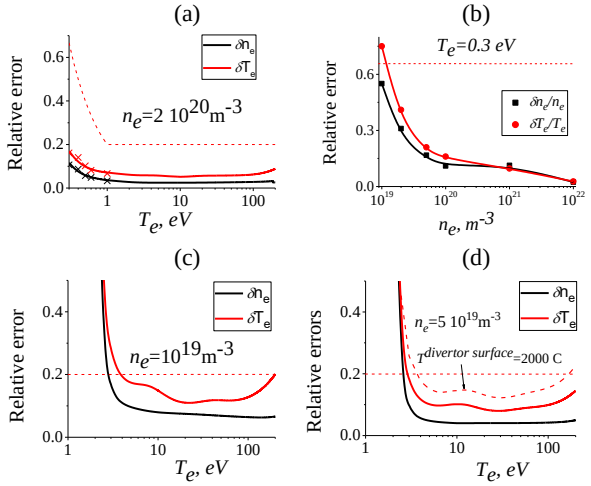

Figure 11. Relative measurement errors of n_e and T_e for data given SOPLS 4.3 run #1514 yielding peak power flux densities of 8 MW/m^2. Background radiation intensity scaled from matching n_e^2 dependence with 5-fold overestimating. The dashed line marks the acceptable accuracy. (a) $\delta T_e/T_e$ under n_e=2·10^{20} m^{-3}. Solid curves are analytical approximation, crosses – errors estimated in numerical experiment; (b) $\delta n_e/n_e$ under T_e=0.3 eV; (c) $\delta T_e/T_e$ under n_e= 10^{19} m^{-3} - the minimum density from the technical requirements; (d) $\delta T_e/T_e$ under n_e= 5·10^{19} m^{-3} - the minimum density. The curve dashed line - when the blackbody radiation for divertor tiles temperature 2000 C is taken into account.

The most important divertor plasma parameter is the degree of plasma detachment/attachment to divertor targets. Detachment requires ion–electron recombination in the plasma volume and this in turn requires the achievement of very low plasma temperatures (<1 eV) at which there is a transition from ionizing to recombining conditions. The ionisation front location does not directly reflect the level of plasma detachment if there is at the same time a vertical displacement of the magnetic configuration, which can occur, for example, as a result of control errors or plasma instabilities. If these two effects can be sufficiently deconvoluted, it is possible to envisage the DTS as a potential sensor in a control loop designed to affect the degree of detachment. The profiles of T_e along the DTS probing chord #1 are shown in Figures 12. Arbitrary vertical shifts of −50 mm, 0 and +50 mm have been applied to the profiles, simulating strike point movements. The Figure 12b shows that the ratio of areas under curve taken for the upper and lower regions of the probing DTS chord gives a matrix of points representing the extent of movement and ionization front position. An operational diagram of this type could be envisaged as a way in which the peak heat flux could be controlled by DTS.

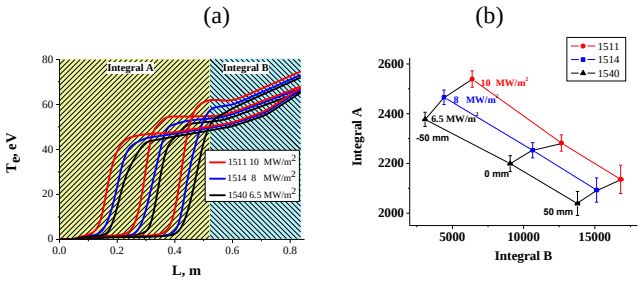

Figure 12. (a) Simulated DTS T_e profiles obtained from SOLPS plasma boundary simulations for differing degrees of detachment and, hence, peak stationary target power flux density (10, 8 and 6.5 MW/m^2) and vertical shifts of the magnetic configuration -50 mm, 0 and +50 mm; (b) Relationship between areas under curve of the lower (Integral A) and the upper (Integral B) parts of T_e curves. The run numbers #1511, 14, 40 are internal identifiers for the SOLPS simulations and the coordinate L represents distance along the probing chord.

In the presence of inaccessible components (e.g. vacuum windows, mirrors inside the vacuum system), the spectral characteristics of the in-vessel optical components, which may change with time, have to be calibrated. For DTS, the procedure must include relative calibration for the temperature, to validate the relative spectral response curves and avoid incorrect measurement of the TS spectrum shape, and absolute calibration for the density, which requires absolute sensitivity. The relative calibration of slowly varying spectral transmission is done comparing in different spectral channels the TS signals from two laser wavelengths (Mukhin E. , 2014). The spectral channels used for measurements in the 5 eV–500 eV range can be calibrated using ratio of the TS signals from the 1064/1047 nm. If the T_e range will be expanded up to several keV's, e.g. during ELM activity in which toroidally asymmetric structures carrying plasma with temperature characteristic of the H-mode pedestal, the corresponding spectral channels can be can be calibrated using signal ratio of 1064/946 nm.

Recent experiments carried out using two diode pumped Nd:YAG and Nd:YLF lasers have demonstrated a possibility to measure T_e within the range T_e =0.02 – 1 keV. [Kurskiev G.S. et. al. Tech. Phys. Letters, in press], see figure 13. The electro-optical shutters of the lasers were synchronized thus making possible to detect TS signals with time delay of a few tens' nanoseconds. The characteristics of the probing and registration system that was used allow to perform multi-laser TS measurements in a steady-state regime, even for the

case when the spectral characteristic of the collection optics was artificially distorted

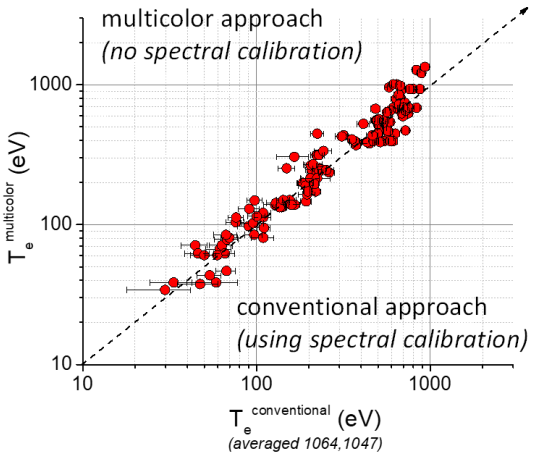

Figure 13. A comparison of the electron temperature measured at the Globus-M2 tokamak measured using multi-laser approach (spectral calibration of the system was not used, Nd:YAG 1064 nm and Nd:YLF 1047 nm lasers with 50 ns time delay) and conventional technique.

The absolute calibration of the diagnostic as a whole, including the entire optical path, should use a light source with known intensity under the same geometry and alignment conditions. The main approach is to use Rayleigh and/or Raman scattering on a gas target. Both have advantages and disadvantages. The main limitation in calibrating by Rayleigh scattering for the DTS is spectrally superimposed stray light. The expected stray light delay is longer than the DTS laser pulse duration (3–4 ns) and, apparently, can be temporally separated. The TS/Rayleigh scattering cross-section ratio for N_2 is 2210 at 1064 nm, which determines the signal value from the gas target with a density of 2.2×10^{16} cm^{-3} (0.8 mbar) equivalent to the TS signal corresponding to $n_e = 10^{13}$ cm^{-3}. The practical advantage of the less intesive Raman compared with Rayleigh scattering is in its broad spectrum, which makes it suitable for both absolute and relative calibration of the spectral channels (see detail in (Mukhin E. , 2014)). Temporal shapes of LIF-derived HeI fluorescence can also be used as an extra method for absolute calibration of the collection system transmission. The fluorescence duration varies from 10 to 100 ns over the ne range 10^{17}-10^{21} m^{-3}, while, that dependence on T_e from 0.3 to 200 eV is much weaker (Mukhin E. , 2019).

A well-known practical problem facing optical diagnostics on large fusion devices, especially in ITER divertor, is the eroded first-wall materials deposited on the front-end optics during normal operation, when shutters are unable to protect. This leads to decreasing diagnostic signals and can result in substantial errors in the interpretation of the data. There are several protecting techniques managing with contamination of the front-end DTS components. The plasma sputtered materials can reach the divertor diagnostic optics during pressure jumps of ~1 ms pulse duration, when plasma blobs with core plasma parameters strike the divertor plates. The eroded material transport by diffusion will be estimated using the Monte-Carlo code KITe (Kinetic Impurity Tracing) (Varshavchik, 2021). The impurity transport caused by convection flows will be minimized by the dust protecting box, situated between plasma and laser launcher following: (1) deviation of the hydrodynamic flow away from the optical axis and (2) absorption/pumping on the box walls (Bukreev, 2014) (Bukreev, 2019) (De Bock, 2016). The front-end laser optics will be thin quartz windows, which have to be self-cleaned by the laser ablation (Razdobarin, 2016) (Mukhin E. , 2009). The front-end collection optic will be cleaned by RF plasma (Mukhin E. , 2011) (Leipold, 2016) (Razdobarin A. , 2015) (Dmitreiv, 2017) (Gorodetsky, 2021) (Shigin, 2021) (Arkhipov, 2011) (Razdobarin A. , 2011) (Gorodetsky, 2020). The innovative diode-pumped Nd:YAG laser 2 J/50 Hz/1064 nm and the auxiliary 1 J/50 Hz/946 nm Nd:YAG and 2 J/50 Hz/3ns Nd:YLF lasers were developed for probing and calibration by TS at the shifted wavelength. The short laser pulse duration helps to reduce both the accumulated plasma background and to separate in time the TS and stray light signals (Kornev, 2019). The digital filter polychromator with ultra-low noise pHEMT based preamplifiers F_{3db}=250 MHz and onboard digitized signal processing system was developed for DTS measurements with probing laser pulses of 3-5 ns. (Makarov, 2021) (Kurskiev G. , 2020) (Zhliltsov, 2020) (Chernakov, 2020) (Mukhin E. , 2012) (Mukhin E. , 2017)

7. LIF in the divertor

Laser-induced fluorescence (LIF) is an active laser spectroscopy diagnostic of atoms/ions in plasma. The technique is based on laser excitation of atom/ion allowed transitions and subsequent registration of fluorescent signals. LIF allows measuring of densities (n_a, n_i) using corresponding collision-radiative models (CRM) and information about electron temperature (T_e) and density (n_e) in the spatial points. Other types of LIF measurements are related to pumping spectral line scanning with a narrowband tunable laser: temperature of the atoms/ions from Doppler broadening, projection of the particle velocities from Doppler shift, the magnetic field from Zeeman splitting etc.

The LIF diagnostic shall measure helium density (n_{He}) and ion temperature (T_i) in ITER divertor according to the requirements specified in Table 3. The main role of LIF is to measure helium density distribution, characterizing the

efficiency of the helium ash removal. In combination with a vacuum pumping system data and gas analyzer, LIF allows monitoring the helium ash level in the main plasma. Besides this, LIF is a backup diagnostic used for measurements of T_i. In combination with a divertor impurity monitor, which is the primary T_i diagnostics, LIF allows knowing the ion temperature distribution along the probing chords. The T_i distribution is essential for evaluating pressure balance in the divertor plasma (Gorbunuv, 2017).

Table 3. LIF measurement requirements

	Range	Frequency	Accuracy
n_{He}	$10^{17} – 10^{21}$ m^{-3}	50 Hz	20%
T_i	0.3 – 200 eV	50 Hz	20%

The diagnostic is combined with a divertor Thomson scattering (DTS) by using common laser-injection and signal collecting optics. The beams will be launched into the outer leg of divertor close to the separatrix with laser mirrors arranged beneath the divertor cassettes (figure 10). Both the DTS and LIF signals will be collected through the gap between neighboring divertor cassettes providing more than 20 independent spatial points. Separation of LIF and DTS signals will be carried out in the diagnostic room with selective mirrors transmitting LIF and reflecting DTS spectral range. The similar measurement chords of LIF and DTS allow using n_e and T_e from DTS for evaluation of n_{He} with CRMs from LIF signals.

The LIF allows measuring both helium atoms (n_{HeI}) and hydrogen-like ions (n_{HeII}) densities. The measurements of n_{HeI} can be realized by two spectroscopic schemes: a triplet – laser pumping the 1s2s ^{3}S → 1s3p ^{3}P transition (388.9 nm) and viewing fluorescence in 1s3d ^{3}D → 1s2p ^{3}P (587.6 nm), and a singlet – pumping 1s2s ^{1}S → 1s3p ^{1}P (501.6 nm) and viewing 1s3d ^{1}D → 1s2p ^{1}P (667.8 nm) (Gorbunuv, 2017) (Munoz Burgos, 2019).

He_{II} ion has a hydrogen-like structure of excited states limiting a set of spectroscopic schemes suitable for LIF. A new laser-induced quenching (LIQ) approach was developed for diagnostics of hydrogen and hydrogen-like ions (Gorbunuv, 2017) (Gorbunuv, 2019). LIQ for He_{II} is based on quenching the most intense line in the visible range 468.6 nm ($n = 4 \rightarrow 3$ transition) by laser pumping to the upper $n = 5$ state (transition $n = 4 \rightarrow 5$, line 1012.3 nm).

1 kHz pulsed optical parametric oscillator (OPO) is suitable both for n_{HeI} (LIF) and n_{HeII} (LIQ) measurements. Figure 14 shows the expected measurement accuracy for DT and Helium scenarios of ITER. OPO gives n_{HeI} and n_{HeII} relative errors <20% in the lower and middle parts of the probing beam, where $n_{HeI} > 10^{17}$ m^{-3}.

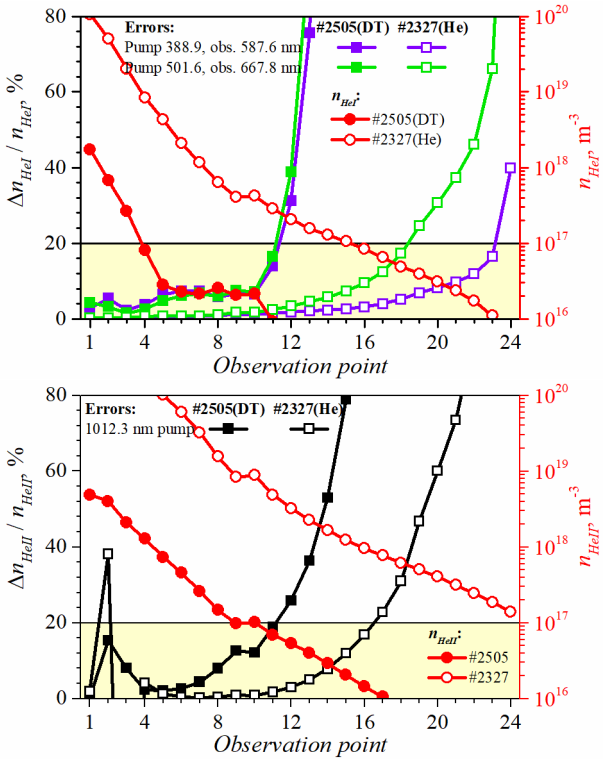

Figure 14. Relative errors of n_{HeI} (top) and n_{HeII} (bottom) measurements (left ordinates) and n_{HeI}, n_{HeII} densities respectively (right ordinates) for #2505(DT) and #2327(He) SOLPS runs

Measurements of the ion temperature can be carried out on the main DT plasma impurity – helium ions. The measurement requires tunable laser with a spectral width of about 10 times narrower (at least) than the absorption line width. The signal-to-noise ratio (SNR) for the T_i should be higher than for density measurements. A short-pulse laser (like OPO) doesn't provide the required SNR, thus, the time-modulated laser is proposed to achieve the accuracy by the signal accumulation over the long time. The transition $n = 4 \rightarrow 5$ (1012.3 nm) is chosen for 468.6 nm He_{II} line quenching due to minimal required laser power (Gorbunuv, 2019).

CRM calculation of the expected quenching and background signals allows estimating accuracy of the T_i using numerical simulations (Figure 15) for Helium and DT ITER scenarios. The spectral line shapes were simulated considering calculated signals and noise sources. Doppler broadened emission spectra, once separated from Stark and Zeeman broadenings, provide a convenient means of making T_i measurements. The laser beam is linearly polarized to reduce intensity of π- component and of corresponding influence of Zeeman splitting.

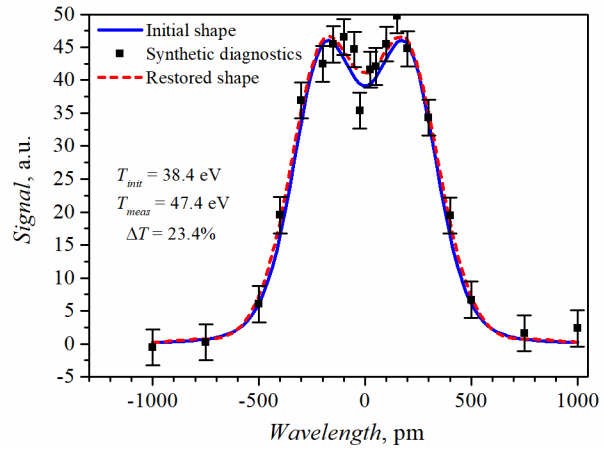

Figure 15. Simulation of the 1012.3 nm HeII spectral line shape for estimation of the T_i measurement accuracy

Results of the ΔT_i estimations are shown in Figure 16. The T_i relative errors were calculated for the LIF/DTS ITER divertor geometry using the following equation: $\Delta T_i = (T_{init} - T_{meas}) / T_{init}$, where T_{init} is the temperature taken from the SOLPS and T_{meas} is determined from the simulated spectral line shape. The simulation was carried out 10^4 times for every observation point. The n_e and T_e (from DTS) were used to consider Stark broadening. Zeeman splitting was estimated for the magnetic field B = 5 T and for the toroidal laser polarization.

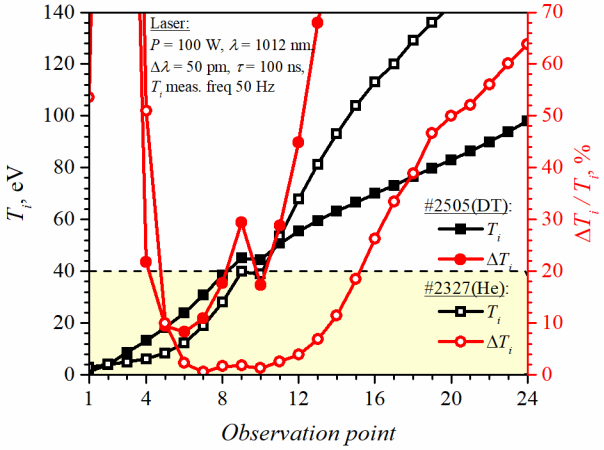

Figure 16. Relative accuracy (right ordinates) of T_i LIQ measurements and T_i distributions (left ordinates)

The calculations show, the ability to measure T_i with relative errors < 20% in the lower part of the probing chord is limited by the pronounced Stark effect. In the upper part of the divertor leg, the measurements are complicated by the low He_{II} ions density.

The LIQ technique can be also applied for hydrogen (deuterium, tritium) diagnostics in ITER divertor (Mukhin E. , 2019). The laser pumping one of the Paschen lines (e.g. P_α = 1875 nm) quenches H_α = 656 nm. Comparing to the conventional LIF for hydrogen with laser pumping and viewing of the fluorescence in H_α, or laser photoionization (LII) of H_β = 486 nm by TS laser, LIQ combines benefits of both LIF and LII. The LIQ requires low-power laser and allows spectral line scanning based measurements like LIF. The wavelength shift of detected radiation versus pumped transition reaches hundreds of nanometers and the laser stray light can be easily blocked as well as in LII.

The CRM assessments of hydrogen density LIQ diagnostic in ITER divertor show possibility to measure $n_{HI} > 10^{17}$ m^{-3} with relative errors better than 20% by 1 kHz pulsed OPO. Using a time-modulated narrowband tunable laser allows scanning of the pumping P_α = 1875 nm spectral line shape. Therefore, LIQ gives the possibility to measure local n_H/n_D, n_D/n_T ratios.

LIQ diagnostics of hydrogen atoms was already tested at Globus-M tokamak. The H_α signal was suppressed by laser radiation with λ = 1005 nm exciting transition $n = 3 \rightarrow 7$ (using OPO laser: $\Delta\lambda$ = 2000 pm, τ = 10 ns, E = 2.2 mJ). As well as OPO, the time-modulated fiber laser with λ = 1875 nm, $\Delta\lambda$ = 1200 pm, P_l = 5 W and repetition rate of 1 MHz was specially designed and manufactured for the n_{HI} measurements in SOL and divertor plasma of Globus-M. The experiments show possibility of measuring $n_{HI} > 10^{16}$ m^{-3} averaging quenching signals over 10 ms in SOL plasmas.

Another useful approach of the LIF in ITER is the electron density measurements basing the analysis of HeI fluorescence pulse shapes (Mukhin E. , 2019). The CRM developed for n_{HeI} describes the temporal behavior of the fluorescent signals depending on the laser pulse shape, exciting transition and local values of n_e and T_e. Particularly, LIF can be used to measure n_e in the range of $10^{17} – 10^{21}$ m^{-3} under T_e = 0.3 – 200 eV by using pulsed OPO laser.

The CRM simulation shows that the fluorescence duration (FWHM) varies from 10 to 100 ns over the n_e range of $10^{17} – 10^{21}$ m^{-3} while dependence on T_e in the range of 0.3 – 200 eV is much weaker. The lower limit of $n_e > 10^{17}$ m^{-3} is determined by reduced dependence on n_e since relaxation of the excited level and hence the fluorescence signal duration is determined mainly by spontaneous emission. Test measurement of n_e was carried out in Globus-M tokamak using TS collection optics. The LIF signal temporal shape satisfy $n_e = (2.00 \pm 0.65) \cdot 10^{19}$ m^{-3} that correlates well with the TS-data $n_e = (2.4 \pm 0.2) \cdot 10^{19}$ m^{-3}.

Comparison of n_e by LIF with n_e by DTS, which depends on the collection system transmission, can also be used as an extra method for absolute *in-situ* calibration of the collection optics transmission in ITER.

8. Toroidal Interferometer-Polarimeter (TIP)

The primary system planned for real-time density control in ITER is the five channel combined toroidal interferometer and polarimeter (TIP). TIP will also contribute to density

profile reconstruction and play a secondary role as a diagnostic of core density fluctuations (Donne, Costley, & Barnsley, 2007). Initial design studies of the TIP were carried out in 1998 (Carlstrom, 1998) and, in 2013, a more detailed design was published (Van Zeeland, 2013) following the successful CDR at ITER. The TIP presented at the CDR featured a traditional two-color vibration compensated interferometry measurement (Irby, 1988) (Carlstrom T. N., 1988) (Kawano, 1996) (Innocente, 1997) (Gil, 2008) with the 10.59 μm CO_2 and 5.42 μm CO laser lines combined with a 10.59 μm CO_2 polarimetry measurement of Faraday rotation using the R and L-wave technique (Dodel & Kunz, 1978) (Rommers & Howard, 1996) (Brower, 2001). Following prototyping activities, it is now envisioned that the CO laser will be replaced by a 4.6 μm quantum cascade laser (QCL) on ITER (Van Zeeland, 2017).

The two-color interferometry approach on TIP is an established technique that relies on using two separate colinear interferometers operating at different wavelengths to deconvolve dispersive plasma-induced phase shifts and motion induced phase shifts. In the cold-plasma approximation, the line-integrated density from TIP will be given by

$$\int n_e dL = \frac{\lambda_{CO2}}{r_e(\lambda_{CO2}^2 - \lambda_{QCL}^2)}\left[\phi_{CO2} - \frac{\lambda_{QCL}}{\lambda_{CO2}}\phi_{QCL}\right]$$

where r_e = 2.82x10^{15} m, λ_i and ϕ_i are the wavelengths and interferometric phase shifts respectively of each laser. Plasma-induced phase shifts of the 10.59 μm CO_2 laser beams in ITER are expected to be 10^3-10^4 degrees and motion-induced phase shifts will likely be 10^4 Deg. (1mm) or larger (Van Zeeland, 2013). In contrast, the polarimeter measures a phase shift given by

$$\phi_{pol} = 2C_p\lambda_{CO2}{}^2 \int n_e \vec{B} \cdot \overrightarrow{dL}$$

with C_P=2.62x10^{-13} rad/T and B is the local magnetic field, from which the Faraday rotation or field weighted line-integrated density can be obtained. Because polarimeter phase shifts are expected to be less than 180 Deg. (Van Zeeland, 2013) and the magnetic field is known, the inclusion of polarimetry allows the two-color system to recover unambiguously from fringe skips at all densities, up to and beyond the Greenwald limit as well as the potential to use the polarimeter itself for feedback density control.

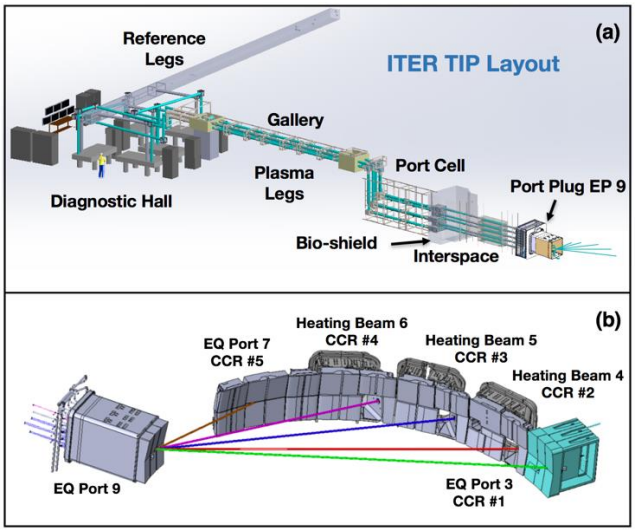

Figure 17. TIP Layout on ITER. (a) view showing TIP layout spanning various zones. (b) TIP chords in ITER vessel and retroreflector (CCR) locations.

The present TIP layout on ITER is shown in Figure 17, where it can be seen that each of the five TIP chords will originate in the diagnostic hall from five independent optical tables. The plasma leg beam lines will be enclosed and transmit each chord to and from the ITER vessel through multiple containment zones. In equatorial port 9 (EP9) an optical labyrinth will transmit each chord through the first wall where they will fan out and be sent to a set of corner cube retroreflectors that are placed in either of the other equatorial ports or neutral beam ducts. The optical train in EP9 features five independent first mirrors and a common first wall hole, to minimize penetration sizes and to reduce risks associated with deposition, erosion and neutron streaming.

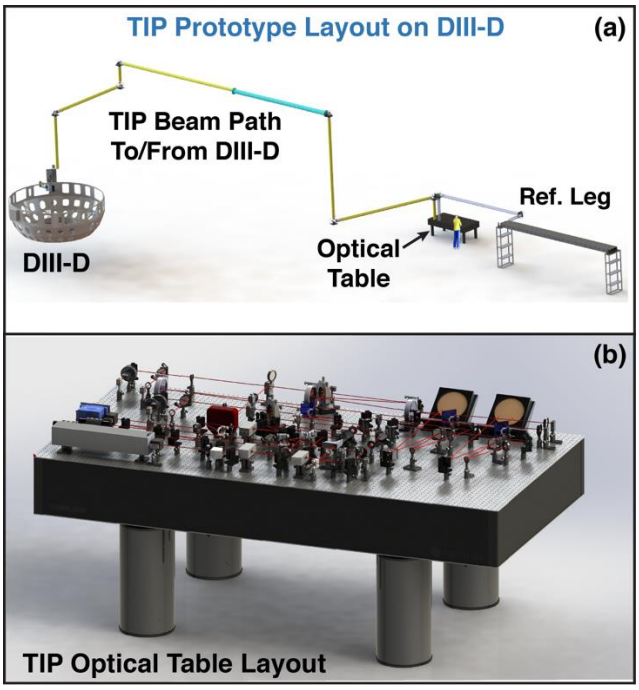

Figure 18. (a) TIP prototype layout on DIII-D. (b) TIP prototype optical table.

While elements of TIP including separate CO2 laser-based two-color interferometry (Carlstrom T. N., 1988) (Kawano, 1996) and R&L-wave polarimetery (Akiyama, 2003) (Van Zeeland, 2008) had been made previously, at the time of the CDR, no previous system had been demonstrated with the combination of characteristics required for TIP, i.e., combined two-color infrared interferometry and polarimetry measurements, long~100 m beam paths and steady-state ~1000s, low-noise measurements. In 2015-2016, a fully functioning TIP lab prototype with the scale of that expected in ITER was constructed and tested (Van Zeeland, 2017). Those tests included several phases, from bench testing to a full 120m beam path with FPGA-based DAQ and a feedback alignment system that was subjected to motions typical of an ITER bake cycle. Over the course of the testing, the initial conceptual design was refined significantly as issues were identified and overcome. As mentioned, a major change was the shift from a CO to quantum cascade laser (QCL) used as the shorter wavelength vibration compensation laser (a 5.22 μm laser in lab tests but planned as a 4.6 μm laser for ITER). Following lab tests, the TIP prototype was moved and installed on DIII-D with encouraging initial results; DIII-D TIP prototype measurements compare well with expectations and the system design is capable of meeting ITER measurement requirements.

The DIII-D TIP prototype layout is shown in Figure 18, where the ~100m roundtrip beam path for the plasma and reference legs are shown in Fig. 18a and the optical table layout in Fig. 18b. A detailed description of the table and components are given in References (Van Zeeland, 2017) and (Van Zeeland, 2018) A key element not shown is the optical table enclosure which reduces airflow, dust and regulates the temperature to help maintain alignment of the components. Like the ITER TIP, the DIII-D prototype features a tangential view and feedback alignment system to keep the system aligned throughout motion associated with pulsed fields during a discharge as well as daily thermal cycles.

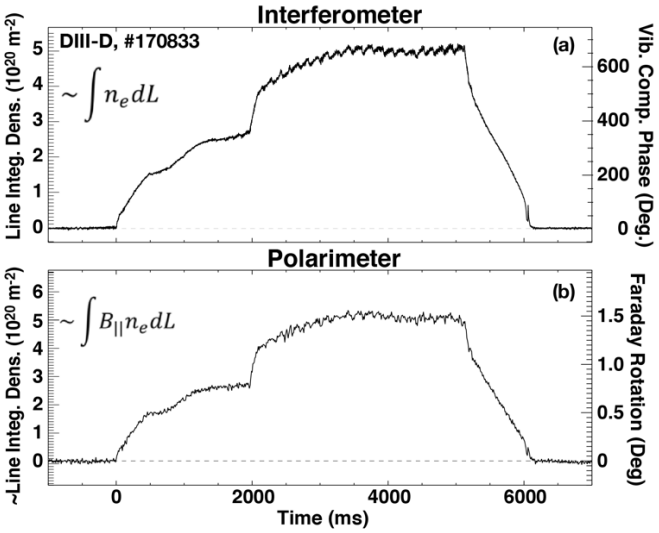

Figure 19. TIP prototype measurements of a DIII-D plasma. (a) Two-color interferometer. (b) Polarimeter.

TIP prototype measurements of a DIII-D plasma are shown in Fig. 19, where the interferometer and polarimeter measurements are shown in Fig. 19a and Fig. 19b respectively along with the measured phase shifts. During DIII-D discharges, the measured phase resolution for the polarimeter and interferometer is 0.05 Deg. (100 Hz bandwidth) and 1.9 Deg. (1 kHz bandwidth), respectively (Van Zeeland, 2018), which are to be compared to the ITER target values of 0.1 and 10 Deg. (Van Zeeland, 2013). The corresponding line-integrated density resolution for the vibration-compensated interferometer is nL = 1.5x10^{18} m^{-2}, and the magnetic field-weighted line-integrated density from the polarimeter is nBL = 1.5x10^{19} Tm^{-2}. Both interferometer and polarimeter measurements compare well to expectations based on calculations using a synthetic TIP diagnostic which takes as inputs Thomson scattering measured density profiles and EFIT magnetic equilibrium reconstructions (Van Zeeland, 2018). As described in Ref. (Van Zeeland, 2018), the TIP prototype active feedback alignment system was essential to obtaining these low-noise data. In addition to line-integrated equilibrium density, 1MS/s TIP prototype data clearly demonstrate the ability to resolve core density fluctuations such as Alfven eigenmodes in the 100 kHz range (See Figure 7 of Ref. (Van Zeeland, 2018)).

While TIP prototype results are encouraging, several open issues and design questions remain. TIP faces many of the

same issues discussed in the context of other laser-based diagnostics discussed in this summary including primarily first mirror degradation. At present, no shutter or mirror cleaning is envisioned, passive mitigation through the use of IR wavelengths, a single small aperture and a novel retroreflector design is the planned approach. An important issue that was identified in testing is atmospheric interaction and specifically, dispersion causing uncompensated interferometric phase shifts due to environmental variation. An example of this effect is given in Fig. 30 of Ref. (Van Zeeland, 2017), where a 0.5 ºC change over ~40 meters of the air-filled beam line caused an uncompensated phase shift of about 25 Deg. or 250% of the TIP interferometer error budget. R&D work will be needed to identify a path forward to handle significant temperature variations but one option includes positive pressure in the beam lines with clean dry air and monitoring temperature variations then removing the uncompesated phase shifts through some experimental fit to the effect. A similar approach has been employed on W7-X (Brunner, 2019). An alternative but difficult approach is the evacuation of the beam lines. Another open issue is the TIP primary vacuum window; leading candidates are BaF_2 and ZnSe. BaF_2 has been used on several devices including the DIII-D TIP prototype, has acceptable transmission and a low Verdet constant; however, it is sensitive to thermal shock and water exposure. While ZnSe is stronger than BaF_2, its higher index of refraction requires an AR coating (which use proprietary coatings with no guarantee of reproducibility) and Faraday rotation in the window must be corrected for to meet polarimeter measurement requirements. Presently, neither window material has been formally approved for use on ITER.

9. Poloidal Polarimeter (PoPola)

Poloidal polarimeter (PoPola) injects thirteen far-infrared (FIR) laser beams (wavelength: 119 μm) into the plasma and measures the polarization change of the FIR laser beams attributed to interaction between the plasma and the FIR laser beams. An equilibrium reconstruction code estimates the profile of plasma current, or equivalently safety factor q(r), by using the PoPola measurement data togther with other diagnostics such as magnetics and CPTS. The q profile is used for physics, real-time suppresion of neo-classical tearing modes and real-time reverse shear control. The design activity has been carried out, and progress has been made, for instance a retroreflector (Imazawa, 2020), a FIR laser, gamma and neutron irradiation tests of a piezo actuator, magneto-optic effect of quartz (window material) (Imazawa R. , 2018), remote alignment method of laser beam position (Imazawa R. , 2018) and passive stabilization of laser beam position (called as “flexible light guide”) (Imazawa R. , 2018). This section focuses on two topics; equilibrium reconstruction taking into account both T_e effect and coupling between the Faraday effect and the Cotton-Mouton effect, and a measurement technique.

The T_e effect and coupling between the Faraday effect and the Cotton-Mouton effect are not mentioned in the previous papers, IPB (Editors, 1999) and Progress in IPB (Donne, Costley, & Barnsley, 2007), but are of significant importance are for discussing the measurement accuracy of q profile identification. Polarimetry involves the measurement of a change in the polarization state, caused by the Faraday effect and the Cotton-Mouton (CM) effect. The Faraday effect mainly changes an orientation angle, θ, of the polarization state and depends on the electron density of plasma, n_e, and magnetic field parallel to probing laser light, $B_{//}$. The CM effect mainly changes an ellipticity angle, ε, of the polarization state and depends on ne and magnetic field perpendicular to probing laser light, $B_{\perp}$. When T_e is high, changes of θ and ε depend on not only B and n_e, but also T_e owing to breakdown of the cold plasma dispersion relation. For burning plasmas such as ITER plasma, the electron temperature is expected to be several tens of keV, and thus the T_e effects on the dispersion relation becomes important (Mifnov, 2007) (P., 2009). In addition to the T_e effect, the coupling between the Faraday effect and the CM effect needs are also significant in the measurement condition of PoPola. Finally, the change of θ and ε are not expressed by using simple line-integral form, but a vector differential equation called a Stokes equation. So, it was an open question whether the q profile can be reconstructed with required accuracy (10 % (Reichle, Ulysse, Casoria, & Turnyanskiy, 2020)) when the T_e effect and the coupling between the Faraday effect and CM effect are not negligible. The authors performed simulations to clarify whether the required accuracy of 10 % is achievable. The PoPola design team demonstrated for the fist time that the q profile can be reconstructed even when the governing equation for the polarization change is given by the complex vector differential equation (i.e. Stokes equation) (Imazawa R. , 2011). The PoPola design team found that the required accuracy of 10 % can not be met in the case of the steady state scenario of ITER plasma operation when the T_e effect is not taken into acount. Thus, the Stokes equation taking into account the T_e effect needs to be solved for reconstructing the q profile. Moreover, it was found that the accuracy of q profile reconstruction using both θ and ε are higher than that using just θ. This is because the data of ε includes the information of the poloidal magnetic field because of the coupling and also includes the information of the toroiodal magnietc field caused by the plasma current. Although the measurent of ε was originally proposed for measuring line-averaged electron density, the measurent of ε is now implemented by PoPola for improving q-profile identification. The study regarding the q-profile

identification leads to the specification of PoPola, which is that the measurement accuracy of θ and ε are 1° and 6°, respectively, and target to 0.1° and 0.6°, respectively.

The next topic is about the measurement technique. This is one of future works that was listed in the Progress in IPB (Donne, Costley, & Barnsley, 2007). The PoPola design team examined the four techniques; the rotating waveplate method, the dual PEM (photo-elastic modulator) method, the Dodel-Kunz method and JET polari-interferometer method. The rotating waveplate method was selected as the preferred option. The major reasons of the selection is the applicability to the wavelength of 119 μm, the capability of measuring the ellipticity angle (ε), the robustness to the deformation of in-vessel mirrors, mechanical vibration and the instability of laser frequency. This section explains only the selected method, and detailed information about the other methods is reported in Reference (Imazawa R. , 2014). The rotating waveplate method consists of a rotating quarter waveplate and a linear polarizer. Detector signal is modulated by the rotation of the quarterwave plate and Fourier analysis of the detector signal provides information identifying the polarization state. It is a well-known technique in the field of polarimetry, but there was no previous experience of measuring at the required time resolution of 10 ms in real time. The theory of the rotating waveplate method is simple and well-known, but practical application with high accuracy is not simple under non-ideal conditions such as concentric distribution of birefringence and non-flatness and wedged shape of the waveplate. The applicability of the rotating waveplate method to PoPola was demonstrated by using both He-Ne laser and quarter waveplate of multi-order retardation (Imazawa R. , 2016). No drift of measurement data was found for 1,000 seconds. The achieved time resolution was 3.3 ms, and the achieved precision of the orientation angle, ellipticity angle, and the Stokes parameter was 0.33°, 0.096°, and 1.2%, respectively. This error will be reduced by using the FIR laser because the error is attributed the run-out of the rotating waveplate, and the run-out normalized by wavelength of FIR laser is much smaller than that of He-Ne laser.

10. Expanded Measurement Capability Potential for PoPola

Since publication of the Progress in IPB (Donne, Costley, & Barnsley, 2007), two new measurement capabilities have been identified as possible for PoPola: (1) internal magnetic field fluctuations and (2) plasma vertical position.

A. Internal magnetic fluctuation measurement

Interest in internal measurements of magnetic fluctuation and non-axisymmetric 3D effects in ITER have significantly increased, due to needs of early detection of disrupting MHD instabilities (Eidietis, 2021) and predictions of unstable electromagnetic turbulence in ITER relevant plasmas (Terry, 2015). Internal magnetic fluctuation measurements, a capability not available from any currently planned ITER diagnostic, may be the key to address these issues. Recent advances in polarimetry have shown that magnetic fluctuation measurements can be accomplished by using the R- and L-wave technique (Brower, 2001), which is also employed for the ITER TIP diagnsotic described in section 8. The technique can detect the Faraday effect with low noise at sub-microsecond time scale, enabling measurements of Faraday effect fluctuations. The noise can be further reduced by using two detectors at each chord to suppress electronic noise via the application of correlation techniques (Chen, 2021). The Faraday fluctuation measured via a horizontal radial chord near the plasma magnetic axis is dominated by magnetic fluctuations along the chord (Ding, 2003), providing a direct internal magnetic fluctuation measurement. In addition, electron density fluctuations along the same chord can be simultaneously measured by adding a local-oscillator (Brower, 2001). By using the R- and L-wave technique for chords at or near the magnetic axis, broadband magnetic turbulence (100-500 kHz) is observed in ELMy H-mode DIII-D plasmas, shown in fig. 20, which correlates with a density ramp and pedestal performance degradation (Chen, 2021). Determined by the probe beam width (~6 cm), the similar measurements on ITER would be sensitive to low-k ($k\rho_s$<~0.1 for a 10 keV plasma in ITER) plasma instabilities, such as electron drift waves, MHD and fast ion driven instabilities.

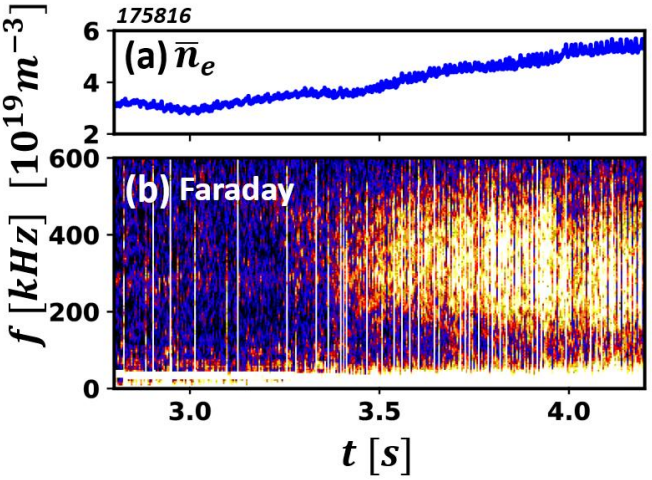

Figure 20 Faraday-effect polarimeter using R- and L-wave technique observed magnetic turbulence during a density ramp in a DIII-D H-mode discharge: (a) line-averaged electron density; (b) spectrogram of Faraday fluctuation measurement of magnetic turbulence.

For PoPola, to achieve the magnetic flucuation measurement capability, one would need to implement R- and L-wave technique for the chord(s) nearest the magnetic

axis. This can be done without compromising PoPola's primary mission to determine the q-profile. There are two possible approaches. First approach is to combine rotating waveplate method described in section 9 and R- and L-wave technique, as illustrated in fig. 21. Beam ω_0 with linear polarization is the probe beam for the rotating waveplate method and generated directly by laser. The probe beams of the R- and L-wave technique, beams ω_R and ω_L with counter-rotating circular polarizations, can be generated either by additional lasers with ~10 MHz frequency difference from ω_0, or by splitting a portion of the ω_0 beam and shifting frequency using an acousto-optic modulator. The rotating waveplate and R- and L-wave methods are integrated by combining all the probe beams together before leaving the optical table, and splitting the return beams into two parts while preserving their polarizations. By appropriately separating the probe beam frequencies, the presence of beam ω_0 will not affect the R- and L-wave measurements. The presence of beams ω_R and ω_L do affect the rotating wave plate measurement, which is avoidable, e.g. by chopping beam ω_R and ω_L periodically: a clean rotating waveplate measurement is accomplished when beams beam ω_R and ω_L are blocked. The chopping frequency is optimized so that good rotating waveplate measurement at the millisecond scale and R- and L-wave measurement at the microsecond scale are realized. Another approach is to only use the R- and L-wave technique for the desired chord(s) near the magnetic axis. In this approach, the R- and L-wave measurement would also provide the q-profile constraint. A potential concern is that non-negligible contamination from Cotton-Mouton effect in the R- and L-wave measurement (Imazawa R. , 2016) (Chen J. , 2018) may affect accuracy of q-profile. However, this concern is largely alleviated by realizing that the absolute error due to the contamination is small (sub-degree level) for chords near the magnetic axis.

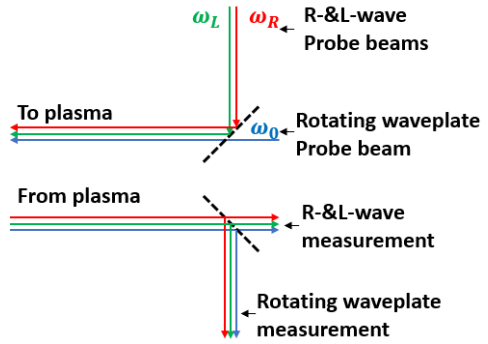

Figure 21 Layout for combination of R- and L-wave technique and rotating waveplate method in PoPola

B. Plasma Position Measurement

Nine chords of the PoPola system view the plasma horizontally from a equatorial port and can therefore be exploited to provide a measurement of the plasma vertical position. Plasma vertical position is determined by the magnetic axis where the radial magnetic field goes to zero and horizontal position is determined by the magnetic axis where the vertical magnetic field goes to zero. To directly measure the radial magnetic field, the double-pass, radially-viewing, PoPola system can be used.

The plasma vertical position, Z_F, can be related to the Faraday measurements, ψ_F, via $Z_F=-\psi_F(0)/\psi'_F(0)$, where $\psi'_F(0)\approx\Delta\psi_F/\Delta z$ (Ding, 2018). The equation gives the center position of the innermost flux surface, Z_F, directly from the Faraday rotation measurement. The ψ'_F is calculated from the slope $\Delta\psi_F/\Delta z$ at z=0. This is a simple linear relation between position and Faraday rotation measurements near the magnetic axis, z~0, which provides essential information for a plasma control system. This vertical position is independent of time derivative, therefore, it is NOT subject to noise from long-time integration. Zero-crossing of Faraday effect measurement provides higher sensitivity to vertical position than other methods such as density or soft X-ray emissivity profile measurements. It should be noted that vertical position is determined directly from the two line-integrated measurements and no inversion is needed. This approximation can enhance the capability of performing real-time control since the line-integrated Faraday-effect measurement can have excellent time resolution (especially when using the R- and L- wave approach) and requires no other equilibrium information.

This approach was recently demonstrated on both the EAST (Ding, 2018) and DIII-D tokamaks where horizontally viewing polarimetry chords are available. An example from DIII-D is shown in Fig. 22, where the Faraday measurement agrees well with the EFIT results (using external magtnetics) through a programmed 25 cm vertical position scan. This approach can be used to independently and non-inductively measure the plasma position thereby providing a cross check for flux loop measurements. Since the Faraday measurements are internal to the plasma, they can also be exploited for plasma control related to vertical displacement events or disruptions.

The plasma position, is the ratio of Faraday rotation to its gradient and is therefore insensitive to the Cotton-Mouton effect itself as it largely cancels. This result simplifies use of polarimetry measurements for plasma position sensor in a plasma control system.

Value of a PoPola measurement of plasma position is threefold for ITER; (1) provides an independent, non-inductive measurement of position, (2) can be used to cross check and validate flux loops or serve as a backup in the event of flux loop failure in harsh ITER radiation environment, and (3) can provide an early warning of plasma vertical position changes related to instability or disruption.

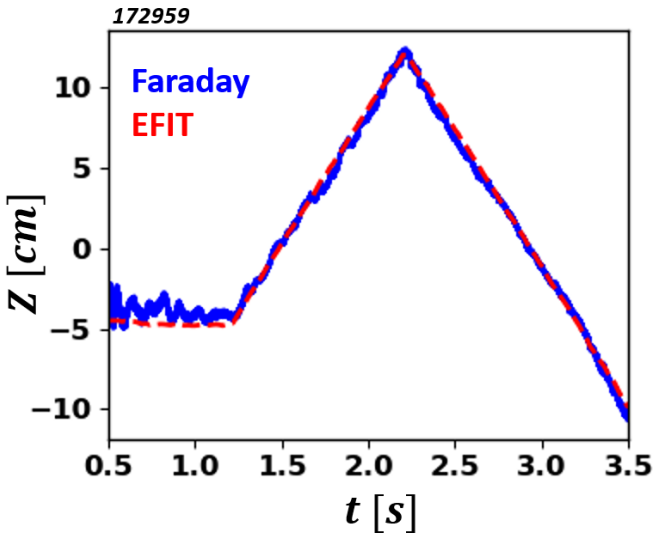

Figure 22 Vertical plasma position on DIII-D showing agreement between Faraday-effect (using 3 central chords) and EFIT results.

11. Dispersion Interferometry for ITER

As described in the previous section, the two-color interferometer approach employed by the TIP can separate the phase shifts caused by a plasma and by mechanical vibrations. Dispersion interferometry (DI) (Drachev, 1993) is a relatively new interferometry configuration and is essentially a variation of the traditional two-color interferometer in that it also uses two different wavelengths. While a standard two-color interferometer measures the phase shift for each wavelength separately, and can solve for vibrations and plasma-induced phase shifts independently, the phase shift measured with DI contains essentially no vibration-induced phase shift, instead measuring the phase shift caused by dispersion of a medium. An additional advantage of DI is a simpler optical configuration. DI uses a single laser source and detector and has no requirement for a path-length matched reference chord.

The concept of DI is shown in Fig. 23. While a standard two-color interferometer is equipped with two laser sources with different wavelengths, DI utilizes a nonlinear crystal to generate the second harmonic component as the second color. The first nonlinear crystal generates the second harmonic component, after which a combination of co-linear fundamental and second harmonic components are launched through the plasma. After passing through the plasma, another nonlinear crystal is used to generate additional second harmonic power and the remaining fundamental component is blocked out. The dispersion interferometer measures the interference between the two second-harmonic beams only. In this approach, the vibration-induced phase shift is optically subtracted, because the two beams experience the same vibrations. In an ideal configuration, the measured phase shift results solely from dispersion through the plasma (Drachev, 1993).

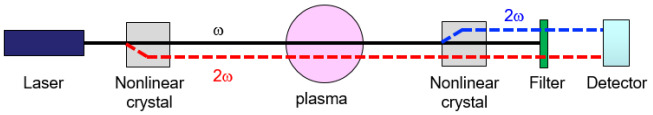

Figure 23: Basic concept of homodyne dispersion interferometer

Starting with a homodyne configuration, several diagnostic techniques like phase modulation (Bagryansky, 2006) (Dreier, 2011) (Akiyama, 2014) (Brunner, 2018) and heterodyne detection (Akiyama, 2018), have been applied to the DI for improvements of time and density resolutions. As an example, the DI configuration on LHD is shown in Figure 24. Since DI is relatively insensitive to mechanical vibrations, the optical frame, where most optics were placed, had no vibration isolation and was directly installed to the diagnostic platform in the LHD hall. The laser source was a CO2 laser with a wavelength of 10.6 mm and output power of 7.5 W. The 5.3 mm component was generated using a AgGaSe2 crystal. The LHD DI utilized phase modulation with a photoelastic modulator (PEM) to improve the density (the phase) resolution. The probe beam injected into the LHD vacuum vessel was reflected by a corner cube mirror installed inside the LHD vessel. The reflected probe beam returned to the optical frame, and was detected. The detailed evaluation method of the plasma phase shift and the electron density is described in Ref (Akiyama, 2014). The line density resolution, which was defined as the standard deviation of a 3 s-long signal acquisition, was 2.5×10^{17} m^{-2} (0.6 deg.), with a response time of 0.1 ms. The measured electron density showed good agreement with the far infrared laser interferometer. The response time was good enough to measure rapid density increases due to pellet injection (Akiyama, 2014).

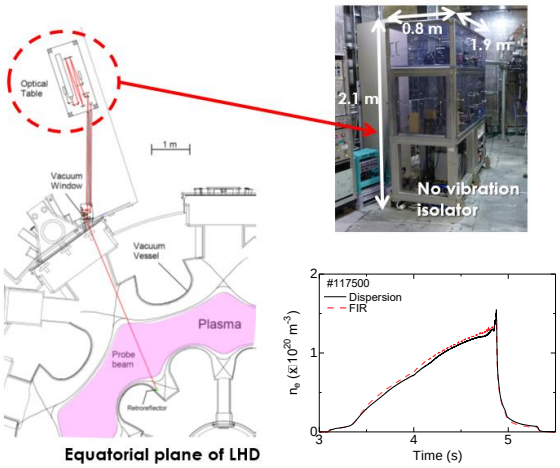

Figure 24: Dispersion interferometer on LHD

The relatively simple configuration of a DI reduces its maintenance and the risk of components failure. The absence of a reference leg makes the system's footprint smaller enabling integration into limited spaces. Advantages of the DI like excellent line density resolution, ease of integration and reliability are reported from several devices, such as TEXTOR (Bagryansky, 2006) (Dreier, 2011), LHD (Akiyama, 2014), W7-X (Brunner, 2018), and DIII-D (Akiyama, 2018). They motivated the inclusion of DI in the ITER diagnostic set. Figure 25 shows a conceptual view of Density Interferometer Polarimeter (DIP) on ITER. DIP is a CO2 laser-based phase modulated DI combined with a polarimeter using PEMs. As with TIP, the polarimeter is incorporated in order to compensate for fringe skips, should they occur. The fundamental component, which is typically filtered out after the 2nd nonlinear crystal, is used for the polarimetry measurements. A PEM-based polarimeter has been previously demonstrated on JT-60U (Kawano Y. , 2001) and does not affect DI measurements, since it measures the polarization angle of the wavelength components which is not used finally in the standard DI. The combination of the DI and the PEM polarimeter was tested on a bench as shown in Figure 25. In the prototype DIP, simultaneous measurements of the interferometer phase shift and the polarization angle were successfully demonstrated (Akiyama,
2016).

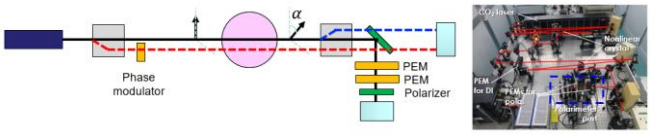

Figure 25: Concept of the combined dispersion interferometer and polarimeter as will be implemented on ITER's DIP

12. Conclusion

Since the ITER physics basis update in 2007, laser aided diagnostics have advanced considerably with many diagnostics going from outline concepts to detailed integrated design solutions ready for implementation.

With this advancement in design many particularly challenging diagnostic components have gone through testing and prototying stages. For example, following prototyping and testing the TIP diagnostic now plans to use a QCL as its' secondary laser as opposed to a CO laser in addition to the main CO_2 laser. The Edge Thomson scattering diagnostic has tested laser beam dump designs for longevity and a new laser beam combiner based on a rotating half-wave plate has been developed. Similarly, demonstration of a rotating waveplate for Popola has been shown to measure Stokes parameters with no drift for over 1000 seconds.

The challenges of the diagnostic designs have lead to development of new hardware. New lasers have been specifically developed for the divertor Thomson scattering diagnostic with diode pumped 2J 50Hz 1064nm main laser and calibrating 1047nm and 946nm lasers with high pulse power and repetition rates. Additionally a digital polychromator design has been developed integrating digitisers within the traditional filter polychromator unit. There are still consider challenges to be overcome, for example the Core plasma Thomson scattering diagnostic would greatly benefit from a free form front optic design. The ability to integrate such a large free form mirror into ITER and shutter and clean it has yet to be demonstrated.

New diagnostic techniques have also been developed since the last ITER physics basis update. Laser induced flourescence has been proposed as a technique to measure Helium density and ion temperature. Similarly laser induced quenching, which pumps individual transition lines using an OPO laser, provides the possibility to measure the n_H/n_D and n_D/n_T ratios. Existing diagnostics are expanding their remits taking on new measurements. The Popola system is now expecting to measure plasma vertical position and magnetic fluctuations. Dispersion interferometry is also proposed which using a simple optical configuration can provide phase shift measurements without any vibration induced phase shift.

The theoretical basis for measurements is also being advanced. Recent simulations have also shown that the Popola must take into account the T_e effect in order to accurately diagnose the q-profile. While the proposal for polarimetric Thomson scattering is not new, there has been very signficant development in the theoretical basis behind this measurement capability. The development of polarimetric Thomson scattering has been driven by that requirement being highlighted by ITER due to the need to accurately diagnostic high T_e.

Importantly laser aided diagnostic techniques proposed for ITER are being trialled on existing Tokamaks. On Globus-M a 1MHz OPO laser was deployed in order to measure n_e using laser induced quenching. The TIP combined two-color interferometry and polarimetry measurements were first tested in the lab and then installed on DIII-D. The first observation of polarimetric Thomson scattering measurements were recently obtained on JET. Vertical position measurements using Popola were demonstrated on DIII-D. Dispersion interferometery was demonstrated on a wide number of machines including LHD and TEXTOR. One of the key outputs of these tests on existing machines is it shows potential issues that need resolution, for example interferometric phase shifts were observed by TIP due to small temperature differences along the beam path. These lab

demonstrations of advanced diagnostics and techniques on existing machines are crucial to de-risk the laser diagnostic implementation for ITER.

Acknowledgements

This work has been carried out within the framework of the EUROfusion Consortium and has received funding from the Euratom research and training programme 2014-2018 and 2019-2020 under grant agreement No 633053. The views and opinions expressed herein do not necessarily reflect those of the European Commission. The work is supported under EPSRC Grant is EP/T012250/1.

This report supported in part Divertor Thomson scattering by Rosatom (contract - № H.4a.241.19.19.1009) and by Ioffe Institute (Russian Federation state funding assignments 0034-2019-0001 and 0040-2019-0023) was prepared as an account of work for the ITER Organization.

Work supported by the U.S. DOE under Contracts DE-FC02-04ER54698 and No. DE-AC02-09CH11466 with Princeton University. All U.S. activities are managed by the U.S. ITER Project Office, hosted by Oak Ridge National Laboratory with partner labs Princeton Plasma Physics Laboratory and Savannah River National Laboratory. The project is being accomplished through a collaboration of DOE Laboratories, universities and industry.

This work is supported by funds from Grant-in-Aid for Young Scientists (B) (Grant No. 20760584) and by NIFS ULHH027. The views and opinions expressed herein do not necessarily reflect those of the ITER Organization.

The views and opinions expressed herein do not necessarily reflect those of the ITER Organization.

References

Akiyama, T. (2003). *Rev. Sci. Instrum., 74*, 2695. doi:10.1063/1.1564276

Akiyama, T. (2014). *Rev. Sci. Instrum., 85*, 11D301.

Akiyama, T. (2016). *Rev. Sci. Instrum., 87*, 11E133.

Akiyama, T. (2018). *Rev. Sci. Instrum., 89*, 10B105.

Arkhipov, I. (2011). *Journal of Nucl. Materials, 415(1)*, S1210-1213. doi:10.1016/j.jnucmat.2010.09.038

Bagryansky, P. A. (2006). *Rev. Sci. Instrum., 77*, 053501.

Bartlett, D. (1996). Physics issues of ECE and ECA for ITER Diagnostics for Experimental Thermonuclear Fusion Reactors. In R. R. Parker, *Diagnostics For Experimental Thermonuclear Fusion Reactors* (p. 183). Varenna.

Bassan, M. (2016). Thomson scattering diagnostic systems in ITER. *JINST, 11*, C01052. doi:10.1088/1748-0221/11/01/C01052

Brower, D. (2001). *Rev. Sci. Instrum., 72*, 1077.

Brunner, J. K. (2018). *JINST, 13*, P09002.

Brunner, J. K. (2019). *JINST, 14*, P11016.

Bukreev, I. (2014). *Instruments and Experimental Techniques, 57(2)*, 156-165. doi:10.1134/S0020441214020250

Bukreev, I. (2019). *Journal of Physics Conference Series*, 1400:077040.

Carlstrom, T. (1998). *Diagnostics for Experimental Thermonuclear Fusion Reactors 2,*. (P. Scott, Ed.) New York: Plenum Press.

Carlstrom, T. N. (1988). *Rev. Sci. Instrum., 59*, 1063.

Chen, J. (2018). *Plasma Phys. Controlled Fusion, 60*, 085001.

Chen, J. (2021). *Rev. Sci. Instrum.*, 043502.

Chen, J. (2021). *Phys. Plasmas, 28*, 022506.

Chernakov, A. (2020). *Fusion Engineering and Design, 156*, 11158. doi:10.1016/j.fusengdes.2020.111588

Chiocchio, S., & Grosset, K. (2020). *ITER Project Requirements Document.* Private Communication.

De Bock, M. (2016). *Journal of Instrum.*, 08010-P08010. doi:10.1088/1748-0221/11/08/P08010

Ding, W. X. (2003). *Phys. Rev. Lett., 90*, 035002.

Ding, W. X. (2018). *Rev. Sci. Instrum., 89*, 10B103.

Dmitreiv, A. (2017). *Physica Scripta*, 014072.

Dodel, & Kunz. (1978). *Infrared Physics, 18*, 773-776.

Donne, A., Costley, A., & Barnsley, R. (2007). Progress in ITER Physics Basis, Chapter 7. *Nucl. Fusion, 47*, 337-380.

Drachev, V. P. (1993). *Rev. Sci. Instrum., 64*, 1010.

Dreier, H. (2011). *Rev. Sci. Instrum., 82*, 063509.

Editors, I. P. (1999). Chapter 7: Measurement of plasma parameters. *Nucl. Fusion, 39*, 2541.

Eidietis, N. W. (2021). *Fusion Science and Technology*, 738-744. doi:10.1080/15361055.2021.1889919

Gil, C. (2008). *Rev. Sci. Instrum., 79*, 10E710.

Giudicotti, L. (09-06-2017). *Depolarization measurements in ITER Core Plasma TS.*

Giudicotti, L. (2016). Conceptual design of a polarmetric Thomson scattering diagnostic in ITER. *JINST, 11*, C01071. doi:10.1088/1748-0221/11/01/C01071

Giudicotti, L. (2017). Polarimetric Thomson scattering for high Te fusion plasmas. *JINST, 12*, C11002.

Giudicotti, L. (2018). First observation of the depolarization of Thomson scattering radiation by a fusion plasma. *Nucl. Fusion, 58*, 044003.

Goldstein, D. (2003). *Polarised light.* New York: Marcel Dekker Inc.

Gorbunuv, A. (2017). *Fusion Engineering and Design, 123*, 695-698. doi:10.1016/J.FUSENGDES.2017.05.129

Gorbunuv, A. (2019). *Fusion Engineering and Design, 146*, 2703-2706. doi:10.1016/J.FUSENGDES.2019.04.091

Gorodetsky, A. (2020). *Journal of Surface Investigation X-ray Synchrotron and Neutron Techniques, 14 (5)*, 1003-1015. doi:10.1134/S1027451020050298

Gorodetsky, A. (2021). *Technical Physics, 66 (2)*, 288-297. doi:10.1134/S10/63784221020122

Imazawa, R. (2011). *Nucl. Fusion, 51*, 113022. doi:10.1088/0029-5515/51/11/113022

Imazawa, R. (2014). *Proceedings of the 41 st Plasma Physics Conference on Plasma Physics (EPS2014).* Berlin: IOP. Retrieved from http://ocs.ciemat.es/EPS2014PAP/pdf/P5.008.pdf

Imazawa, R. (2016). *Rev. Sci. Instrum., 87*, 013503. doi:10.1063/1.4939444

Imazawa, R. (2018). *Plasma and Fusion Research, 13*, 1405112. Retrieved from http://www.jspf.or.jp/PFR/PDF2018/pfr2018_13-1405112.pdf

Imazawa, R. (2018). *Proceedings of the 27th IAEA Fusion Energy conference (FEC2018)*, (pp. FIP/P1-14). Gujarat, India.

Imazawa, R. (2018). *Rev. Sci. Instrum., 89*, 103104. doi:10.1063/1.5040911

Imazawa, R. (2020). *Fusion Engineering and Design, 155*, 111570. doi:10.1016/j.fusengdes.2020.111570

Innocente, P. (1997). *Rev. Sci. Instrum., 68*, 694.

Irby, J. (1988). *Rev. Sci. Instrum., 59*, 1568.

Kawano, Y. (1996). *Rev. Sci. Instrum., 67*, 1520.

Kawano, Y. (2001). *Rev. Sci. Instrum., 72*, 1068.

Kornev, A. (2019). *Fusion Engineering and Design, 146*, 1019-1022. doi:10.1016/j.fusengdes.2019.01.147

Kurskiev. (2015). A study of core Thomson scattering measurements in ITER using a multi-laser approach. *Nucl. Fusion, 55*, 053024. doi:10.1088/0029-5515/55/5/053024

Kurskiev, G. (2020). *Nuclear Instruments and Methods in Physics Research, 963*, 163734. doi:10.1016/j.nima.2020.163734

Leipold, F. (2016). *Rev. Sci. Instrum, 87 (11)*, 11D439. doi:10.1063/1.4962055

Litnovsky, A. (2010). Development of in situ cleaning techniques for diagnostic mirrors in ITER. *Fusion Eng. Des., 86*, 1780-3.

Makarov, A. (2021). *Applied Optics, 60*, 547-550. doi:10.1364/AO.412905

Mifnov, V. V. (2007). *Physics of Plasmas, 14*, S337-S384. doi:10.1063/1.2790886

Mirnov, V. (2016). Exact relativistic expressions for polarization of incoherent Thomson scattering. *Phys. Plasmas, 23*, 052108.

Mirnov, V. (2017). Polarization of incoherent Thomson scattering for electron temperature measurement",. *Plasma Phys. Control. Fusion, 59*, 063001.

Mukhin. (2012). First mirrors in ITER: material choice and deposition prevention / cleaning techniques. *Nucl. Fusion*, 013017.

Mukhin, E. (2009). *Nucl. Fusion, 49 (8)*, 085032. doi:10.1088/0029-5515/49/8/085032

Mukhin, E. (2011). *Nucl. Fusion, 52 (1)*, 013017. doi:10.1088/0029-5515/52/1/013017

Mukhin, E. (2012). *JINST, 7(02)*, C02063. doi:10.1088/1748-0221/7/02/C02063

Mukhin, E. (2014). *Nucl. Fusion, 54*, 043007. doi:10.1088/0029-5515/54/4/043007

Mukhin, E. (2017). *Fusion Engineering and Design, 123*, 686-689. doi:10.1016/j.fusengdes.2017.06.014

Mukhin, E. (2019). *Nucl. Fusion*, 086052.

Munoz Burgos, J. (2019). *Physics of Plasmas, 26*, 063301. doi:10.1063/1.5088363

Orsitto, F., & Tartoni, N. (1999). Proposal for a new electron temperature diagnostic for fusion reactors. *Rev. Sci. Instrum.*, 798.

P., F. O. (2009). *Plasma Physics and Controlled Fusion, 51*, 065004. doi:10.1088/0741-3335/51/6/065004

Parke, E. (2014). A polarization-based Thomson scattering technique for burning plasmas. *JINST, 9*, C02030.

Pasch, E. (2018). *Rev. Sci. Instrum., 89*, 10C115. doi:0.1063/1.5038422

R, H., & M, B. (2018). *Collection Optics system for ITER Core TS.* ITER Organisation.

Razdobarin. (2016). *IAEA FEC*, MPT/P5-40. Retrieved from https://nucleus.iaea.org/sites/fusionportal/Shared%20Documents/FEC%202016/fec2016-preprints/preprint0766.pdf

Razdobarin, A. (2011). *Fusion Engineering and Design, 86(6-8)*, 1341-1344. doi:10.1016/j.fusengdes.2011.02.052

Razdobarin, A. (2015). *Nucl. Fusion, 55 (9)*, 093022. doi:10.1088/0029-5515/55/9/093022

Reichle, R., Ulysse, A. d., Casoria, F., & Turnyanskiy, M. (2020). *SRD-55 (Diagnostics).* ITER Organisation.

Rommers, & Howard. (1996). *Plasma Phys. Control. Fusion, 38*, 1805-1816.

Scannell, R. (2017). Design advances of the Core Plasma Thomson Scattering diagnostic for ITER. *JINST, 12*, C11010. doi:10.1088/1748-0221/12/11/C11010

Segre. (2000). Polarization of radiation in incoherent Thomson scattering by high temperature plasmas",. *Phys. Plasmas, 7*, 2677.

Shigin, P. (2021). *Fus. Eng. Design, 164*, 112162. doi:10.1016/j.fusengdes.2020.112162

Terry, P. W. (2015). *Nucl. Fusion, 55*, 104001.

Van Zeeland, M. A. (2008). *Rev. Sci. Instrum., 79*, 10E719.

Van Zeeland, M. A. (2013). *Rev. Sci. Instrum., 84*, 043501.

Van Zeeland, M. A. (2017). *Plasma Phys. Controlled Fusion, 59*, 125005.

Van Zeeland, M. A. (2018). *Rev. Sci. Instrum;, 10*, 10B102. doi:10.1063/1.5037461

Varshavchik, L. (2021). *Plasma Physics and Controlled Fusion, 63(2)*, 025005. doi:10.1088/1361-6587/abca7e

Vayakis, G. (2006). Status and prospects for mm-wave reflectometry in ITER. *Nucl. Fusion, 46*, S836. doi:10.1088/0029-5515/46/9/S20

Vayakis, G., & Scannell, R. (2017). *Beam dump for the ITER Core Plasma TS.* ITER Organisation.

Walsh, M. (2006). Design Challenges and Analysis of the ITER Core LIDAR Thomson Scattering System. *Rev. Sci. Instrum., 77*, 10E525. doi:10.1063/1.2336473

Yatsuka, E. (2013). Chevron Beam Dump for ITER edge Thomson scattering system. *Rev. Sci. Instrum., 84*, 103503. doi:10.1063/1.4824141

Yatsuka, E. (2015). Enhancement of resistance against high energy laser pulse injection with chevron beam dump. *Fusion Engineering and Design, 100*, 461-467.

Yatsuka, E. (2016). Development of laser beam injection system for the Edge Thomson Scattering (ETS) in ITER. *Journal of Instrumentation*, C01006. doi:10.1088/1748-0221/11/01/C01006

Yatsuka, E. (2017). Note: Lossless laser beam combiner employing a high-speed rotating half-wave plate. *Rev. Sci. Instrum., 88*, 076107.

Yatsuka, E. (2018). Technical innovations for ITER Edge Thomson scattering measurement system. *Fusion Engineering and Design, 136*, 1068-1072.

Yatsuka, E. (2020). Gamma-ray irradiation effects on optical coatings and polarizers for edge Thomson scattering system in ITER. *Fus. Eng. Design, 160*, 111846.

Zhliltsov. (2020). *Nuclear Instruments and Methods in Physics Research, 976*, 164289. doi:10.1016/j.nima.2020.164289